(2)

Quarterly Letter Report

Growth, Characterization and Device Development in Monocrystalline Diamond Films

Supported by the Innovative Science and Technology Office
Strategic Defense Initiative Organization
Office of Naval Research
under Contract #N00014-90-J-1604
for the period July 1, 1991–September 30, 1991

Robert F. Davis, Jeffrey T. Glass, Klaus J. Bachmann,
R. J. Nemanich* and R. J. Trew**
North Carolina State University
c/o Materials Science and Engineering Department
*Department of Physics
**Electrical and Computer Engineering
Raleigh, NC 27695-7907

September 30, 1991

REPORT DOCUMENTATION PAGE

Form Approved
OMB No 0704-0188

1. AGENCY USE ONLY (Leave blank)	2. REPORT DATE	3. REPORT TYPE AND DATES COVERED
	September 1991	Quarterly Letter 7/1/91–9/30/91

4. TITLE AND SUBTITLE
Growth, Characterization and Device Development in Monocrystalline Diamond Films

5. FUNDING NUMBERS
s400003srr08
1114SS
N00179
N66005
4B855

6. AUTHOR(S)
Robert F. Davis

7. PERFORMING ORGANIZATION NAME(S) AND ADDRESS(ES)
North Carolina State University
Hillsborough Street
Raleigh,NC 27695

8. PERFORMING ORGANIZATION REPORT NUMBER
N00014-90-J-1604

9. SPONSORING/MONITORING AGENCY NAME(S) AND ADDRESS(ES)
Department of the Navy
Office of the Chief of Naval Research
800 North Quincy Street, Code 1513:CMB
Arlington, VA 22217-5000

10. SPONSORING/MONITORING AGENCY REPORT NUMBER

11. SUPPLEMENTARY NOTES

12a. DISTRIBUTION/AVAILABILITY STATEMENT
Approved for Public Release; Distribution Unlimited

12b. DISTRIBUTION CODE

13. ABSTRACT (Maximum 200 words)

Investigations concerned with the out-diffusion of ion-implanted C atoms to the surface of monocrystals of Cu(100) under supersaturated conditions, the use of surfactants such as Ag to reduce the surface energy of the C species and studies involving the diffusion of dissolved C down thermal gradients have resulted in the formation of graphite at the surface or interface of the Cu crystals. Metal contacts of Ti deposited below 400°C have been shown to be rectifying. The Schottky barrier height has been measured by ARUPS to be 1.0±0.2 eV. Deposition or annealing above this temperature results in the formation of Ti-C bonding and the gradual enhancement of ohmic behavior. Studies concerned with the deposition of TiN by RPCVD have been initiated. It has also been shown that processing techniques, both growth and annealing, have a significant effect on the electrical conductivity of diamond films, particularly at low temperatures. Activation energies from 0.1 eV to 1.1 eV (natural diamond=1.4 eV) were measured. Finally the potential for diamond devices in microwave and millimeter wave applications have been extensively examined, the results of which are reported herein.

14. SUBJECT TERMS	15. NUMBER OF PAGES
diamond thin films, chemical vapor deposition, Raman spectroscopy, electronic devices, MESFETs, ion implantation high pressure studies, epitaxial regrowth, amorphous C films	49
	16. PRICE CODE

17. SECURITY CLASSIFICATION OF REPORT	18. SECURITY CLASSIFICATION OF THIS PAGE	19. SECURITY CLASSIFICATION OF ABSTRACT	20. LIMITATION OF ABSTRACT
UNCLAS	UNCLAS	UNCLAS	SAR

Table of Contents

I. Growth of Carbon Films on Monocrystalline Copper (A. Vasudev and R. F. Davis)

A. Background

Prins and Gaigher [1] recently reported that epitaxial diamond layers can be grown on single crystal copper by means of high dose carbon ion implantation at elevated temperatures. The ultra-thin (≈400Å) films were characterized as diamond using a d-spacing determination from transmission electron diffraction patterns. They further claimed from the electron diffraction patterns that the films showed a preferred orientation with respect to the copper substrate. Several months ago Prins retracted his claim of diamond heteroepitaxy on copper. However, recently he has renewed this claim regarding the achievement of diamond by this technique. Recent examination of one of his films at the Naval Research Laboratory using Raman Spectroscopy strongly indicated the presence of diamond. Similar experiments by several investigators in the United States have failed to duplicate Prins' results. Lee et. al. [2] reported that the implantation-outdiffusion mechanism does form single crystal carbon films on copper (100), (110), (111), and (210) substrates, but the films are actually (0001) oriented graphite instead of diamond. They characterized the films using transmission electron diffraction, Raman spectroscopy, and x-ray diffraction. Experiments using ion implantation and annealing parameters related to those used by Prins were also conducted at the Research Triangle Institute (Posthill), the University of North Carolina (Swanson) and NCSU (Vasudev and Davis) to verify the existence of a diamond film on (110) copper, but the results were similar to those reported by Lee. The results obtained by the last investigators are discussed below.

The traditional method of overcoming the problem of an unfavorable growth mode is to restrict the growth kinetics to inhibit islanding. This is done either by decreasing the growth temperature or by increasing the deposition rate. An alternative approach to this dilemma would be to use a surfactant to alter the surface energy and thus the growth mode of the film. By collectively lowering the surface energy of both the substrate and the growing film it could be possible to achieve a Frank-van der Merwe type of growth for the growing diamond film.

Surfactants can be used to alter the surface deliberately by filling the dangling bonds which normally occur on the clean surfaces, thereby creating a stable termination. For a surfactant to work effectively, it must fulfill the following criteria: (i) it must be sufficiently mobile to avoid incorporation at a given growth rate; (ii) it must surface segregate, and (iii) it must reduce the surface energy of both the substrate and the overlayer. Desorption effects must also be considered since a complete surface coverage is needed throughout the nucleation and growth process. The surfactant may also have to

occupy epitaxial sites possibly assisting any exchange mechanism with the incoming growth species. Thus, island formation and interdiffusion are kinetically inhibited without any sacrifice of epitaxy.

Table I lists the candidate materials selected by this author for use as surfactants for the growth of diamond on copper substrates. Silver was the first choice because of its high melting temperature, low vapor pressure, low surface energy relative to copper and lack of solid solubility with carbon and copper. Also no special care in terms of safety is needed during the experiments, in contrast to the candidates of lead and bismuth. These last two materials have higher vapor pressures and lower melting temperatures which further restrict the limits of their use.

Table I. Surfactants on copper substrates.

Element	Solid Solubility in Cu (wt%)	Carbon solid solubility in surfactant	Vapor Pressure (Torr)	Surface Energy ($ergs/cm^2$)
Ag (T_m=961°C)	779°C 8.1 700 4.8 600 2.5 500 1.3 400 0.6 300 0.2 200 <0.1	0.036 at%C @ 962°C	400°C $<10^{-11}$ 500 $2X10^{-10}$ 800 $5X10^{-5}$	1140 ± 90 @ (876-941°C) 1130 @ T_m 1302 @ (25°C)
Pb (T_m=328°C)	no solid solubility below 328°C	limited	400°C $2X10^{-7}$ 500 $3X10^{-5}$ 600 $4X10^{-4}$ 700 $5X10^{-3}$ 800 $5X10^{-2}$	450 @ T_m 534 @ (25°C)
Bi (T_m=272°C)	no solid solubility below 270°C	limited ≈0.0003 wt%C @ 750°C	300°C $1X10^{-9}$ 400 $9X10^{-7}$ 500 $5X10^{-5}$ 600 $1X10^{-3}$ 700 $1.5X10^{-2}$	365 @ T_m 382 @ 25°C

Another possible solution for the growth of monocrystalline diamond films is by the use of the travelling solvent method (TSM) [3]. In TSM, a thermal gradient across a sandwich comprised of a thin layer of solvent (e.g., Pb) located between the source (e.g., graphite) and the seed (e.g., Ni) material. At the appropriate temperature, material is

dissolved at both solvent-crystal interfaces; however, the solubility is greater at the hotter interface. The resultant concentration gradient provides a driving force to move solute through the liquid zone from the hotter to the cooler interface; the latter becomes supersaturated and deposition occurs. This process may continue until the desired amount of deposition is achieved or until the solvent zone has totally dissolved the source material.

Lead is a good solvent material for such a process, since it possesses a low melting temperature and does not form solid solutions with either Ni or graphite, the at low temperatures. By sandwiching the lead between the Ni and graphite, the surface tension should keep the liquid Pb from dripping off. Pb desorption at high temperatures, where the vapor pressure is high, can be reduced by conducting the experiment in Ar rather than in vacuum.

In the approach used in this study, C ions were implanted into single crystal copper (110) substrates at room temperature and were annealed in the presence of a hydrogen plasma. Surfactants were used in some instances to create a stable surface termination in order to facilitate a Frank-van der Merwe type of growth for the growing carbon film. The C out-diffusion was conducted in a controlled manner. X-ray Photoelectron Spectroscopy (XPS), and Auger Electron Spectroscopy (AES) contained in a UHV analytical system were used to characterize the growing carbon film.

B. Experimental

1. Ion Implantation and Annealing

A 99.999% pure, (110) oriented copper substrate, having a diameter of 0.5 inches and a thickness of 1.5mm, was electropolished and cleaned. Carbon-12 ions, obtained from a CO_2 source, were implanted at room temperature with a beam energy, dose and angle of 120keV, 5×10^{17} ions/cm^2 and 10°, respectively. The cleaning procedure, following this implant, included a thirty minute exposure to ultraviolet light to remove the hydrocarbons from the surface and a hydrochloric acid etch to remove the native oxide. Surface carbon present from the implantation procedure was removed with a hydrogen plasma treatment at 300°C for thirty minutes. The samples were characterized using the above mentioned techniques.

2. Surfactants

Silver, 99.999% pure, was the chosen surfactant for the second part of this study. It was thermally evaporated on ^{12}C-ion-implanted-Cu. The Ag film thickness was estimated at ≈40Å. A long exposure to the atmosphere occurred prior to the C exsolution procedure; thus a hydrogen plasma treatment (T≈300°C) was employed to clean the

surface. Silver and Cu were the only elements detected by XPS following this plasma etching treatment. The implanted C was exsolved from the Cu substrate at 550°C in the hydrogen plasma. The tools of XPS and AES were used to characterize the annealed surface.

3. Travelling Solvent Method

Lead, 99.999% pure, was thermally evaporated on (100) oriented single crystal Ni and a polycrystalline, pyrolytic graphite sample. The Pb film thickness, measured by a profilometer, was ≈5500Å. The Pb-covered faces of both the Ni and graphite were mated and placed on a flat tungsten boat in a thermal evaporator, as illustrated below:

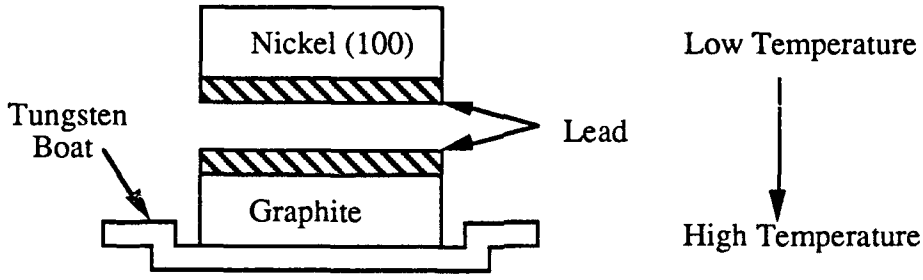

Figure 1. The Travelling Solvent Method with Pb as the solvent.

The graphite substrate and the tungsten boat were in intimate contact throughout the annealing procedure. The tungsten boat was resistively heated, in an Ar-rich atmosphere, to a temperature such that the Pb melted (≈450°C) and was held at this temperature for one hour. Scanning electron microscopy (SEM) was used to characterize the Ni surface.

C. Results & Discussion

1. Ion Implantation and Annealing

An XPS survey scan was performed on the Cu (100) implanted substrate following the UV and HCl cleaning procedures. All of the characterization was conducted *in-situ*, since the sample was never removed from the UHV chamber. The hydrochloric acid effectively removed all of the surface oxide and apparently left the surface hydrogen-terminated. Impurity C on the copper surface was removed before the out-diffusion study was performed. It was deemed necessary to conduct this cleaning step at an efficiently low temperature such that the implanted C atoms in the bulk did not diffuse to the surface of the Cu. This was accomplished by heating the substrate with the help of a hydrogen plasma at 300°C for thirty minutes. An optical pyrometer was used to measure the substrate temperature. The sample was positioned inside the plasma. At 300°C, the C etch rate is faster than its exsolution rate; thus, the surface is left free of any C.

An exsolution temperature of 400°C was selected since it lies in a temperature regime where the etch rate of graphite and the exsolution rate of C to the Cu surface in the H_2 plasma are similar. At the lower temperature of 300°C the H_2 plasma etches the surface graphite readily. By contrast, at 550°C the diffusion of C from the bulk is faster than the etch rate of the graphite by the hydrogen plasma thus resulting in an overgrowth (see Ref. [4]). The much higher temperature of 800°C was also investigated, since it had been reported by Yoder (private communication) that diamond films could be realized in this high temperature regime, if the Cu surface was very clean.

The thesis underlying this approach was that the atomic hydrogen from the plasma would preferentially etch any sp^2 bonded graphite nuclei that formed on the surface leaving behind any sp^3 bonded diamond nuclei, since the sp^2/sp^3 etch rate ratio is ≈100/1. After annealing for 5 hours at 400°C in a hydrogen plasma, the XPS spectra showed the presence of C on the surface. Figure 2(a) illustrates this point. The C_{1s} peak is observed along with the characteristic Cu peaks intensity. The absence of a carbide peak indicates that the bonding between the C and Cu is weak, a necessary condition for diamond growth by the implantation-outdiffusion method proposed by Prins.

Auger electron spectroscopy was used to identify the carbon polymorph present on the surface. In this case, the C present was identified as pyrolytic graphite (sp^2 bonding), since the C(KLL) fine structure, shown in Figure 2(b), has the highest intensity peak at a lower binding energy. By contrast, for diamond, the highest intensity peak should be at a higher binding energy due to the sp^3 bonding. Similar results were realized for an annealing temperatures of 800°C as shown in Figure 3.

None of the surfaces from these experiments had sufficient details such that features could be resolved by SEM. The presence of atomic hydrogen during the anneal invariably etched a large portion of the exsolved surface C leaving a few monolayers at most on the surface.

2. Surfactants

The XPS survey scan (shown in Figure 4) was obtained following the H_2 plasma clean. The only elements detected were Ag, and Cu. The next step was to activate the C atoms within the Cu lattice such that they out-diffused to the Cu-Ag interface. This procedure was conducted in the H_2 plasma at 550°C in a similar manner as the procedure described above in Part I-C-1. The XPS results showed the presence of Cu and C but the Ag peak had disappeared. It is believed that at 550°C and in the presence of a hydrogen plasma the Ag was lost as a result of etching from the surface rather than by diffusion into the Cu bulk.

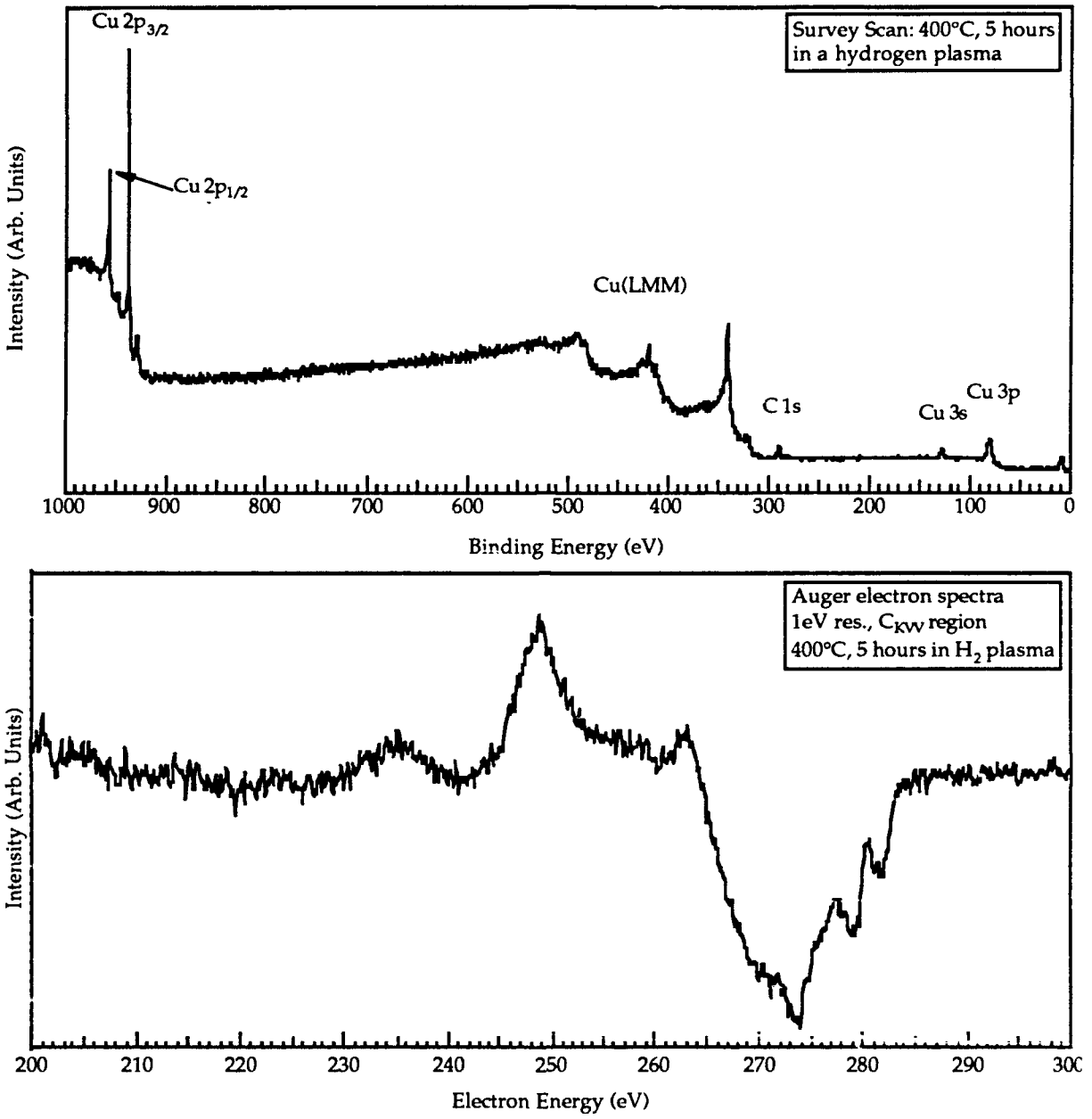

Figure 2. (a) XPS and (b) AES spectra of a copper surface following a 400°C, 5 hour anneal in a hydrogen plasma. These spectra verify the presence of carbon on the surface in the form of graphite.

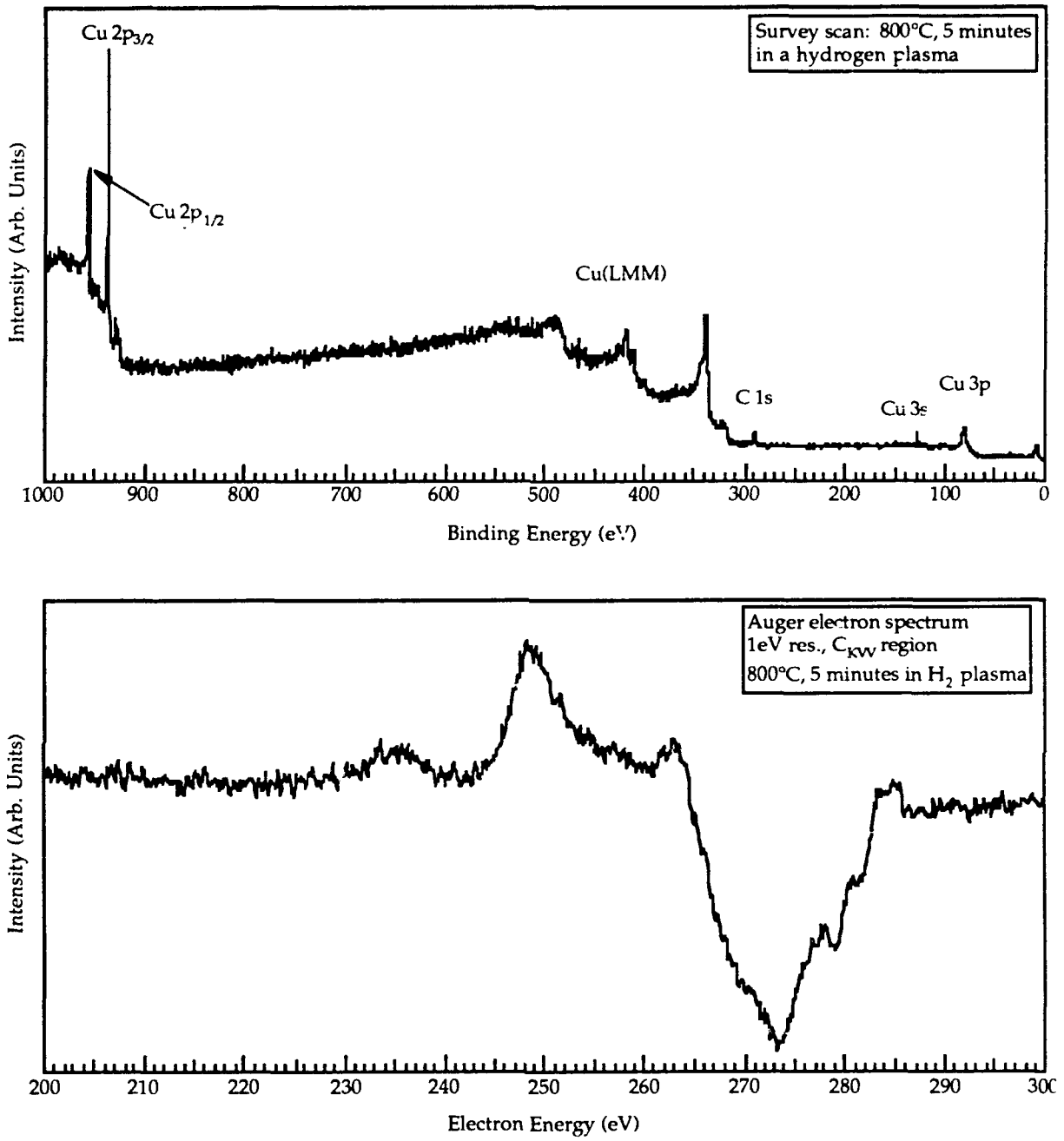

Figure 3. (a) XPS and (b) AES spectra of a copper surface following an 800°C, 5 minute anneal in a hydrogen plasma. These spectra verify the presence of carbon on the surface in the form of graphite.

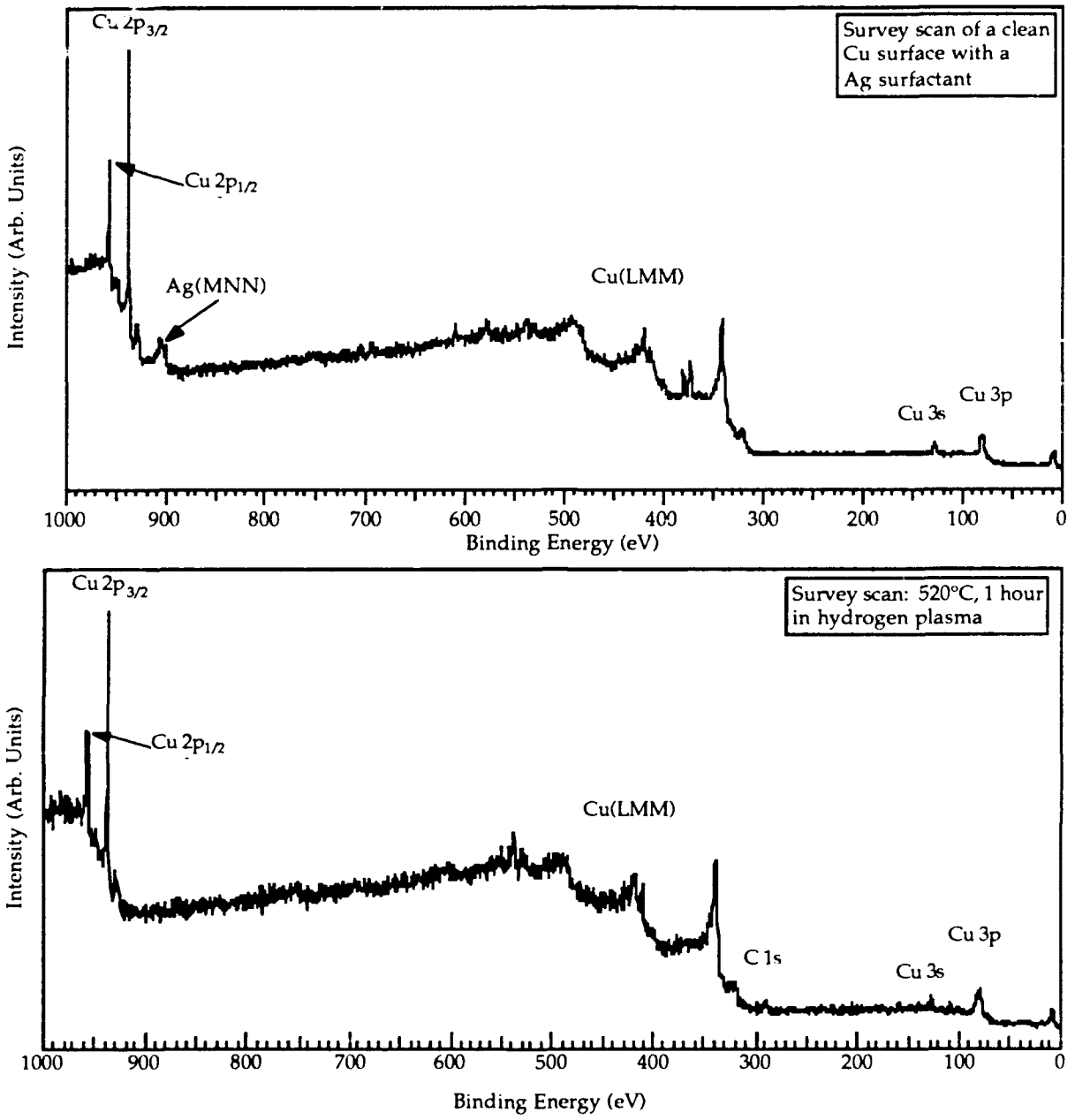

Figure 4. XPS spectra of (a) Ag on a clean copper surface after a 300°C hydrogen plasma clean but before a 520°C anneal; (b) Post 520°C anneal: Ag is no longer present on the surface. Also, the ion implanted C has out-diffused from the bulk.

3. Travelling Solvent Method

The only surface phase seen on the (100) oriented Ni were droplets of Pb. No platelets or flakes of graphite or diamond were observed anywhere on the Ni surface. Perhaps 450°C is not a sufficiently high temperature for the graphite to dissolve into the

Pb. It may also be that a sufficiently thermal radiant was not established to cause the atomic C to diffuse through the Pb to the Ni. Results from a higher temperature anneal and/or steeper thermal gradient must be obtained to determine if this idea has any merit for the growth of diamond films.

D. Conclusions

All of the experiments performed in this study resulted in a graphitic surface phase. An effective cleaning method, as by XPS, has been established for removing the surface impurities C and O. The exsolution of C from Cu (100) occurs even at 400°C. Silver was used as a surfactant but was lost during the 520°C anneal in the hydrogen plasma. Perhaps annealing in-vacuo or in Ar could solve this desorption problem. Deposition of C on Ni did not occur using the travelling solvent method.

E. Objectives

The research for the next reporting period will continue to have as its objective, the formation of monocrystalline diamond on non-diamond substrates such as single crystal Cu. Additional implantation studies through a graphite grid into Cu(100) and Cu(110) followed by outdiffusion will be investigated. In addition, fine line deposits of graphite will be produced followed by the outdiffusion of the implanted C. In this way, the edge of the graphite flakes in the deposited lines may be used as a nucleation sites. Work regarding surfactants and the traveling solvent method will also continue.

F. References

1. J. F. Prins, H. L. Gaigher, "A TEM Study of Layers Grown on Copper Using Carbon-Ion-Implantation," in *New Diamond Science and Technology*, R. Messier, J. T. Glass, J. E. Butler and R. Roy, Eds.,. Materials Research Society, Special Conference Edition, 1991, pp. 245-251.
2. S.-Tong Lee, Samuel Chen, G. Braunstein, X. Feng, I. Bello, and W.M. Lau, "Heteroepitaxy of Carbon on Copper by High-Temperature Ion Implantation," Appl. Phys. Lett. **59** 7, 785 (1991).
3. J. D. Hong, R. F. Davis, "Deposition of Diffusion Tracers on SiC Using a Travelling Solvent Zone," Materials Science and Engineering, **33**, 145 (1978).
4. R. F. Davis, K. J. Bachmann, J. T. Glass, R. J. Nemanich and R. J. Trew, "Growth, Characterization and Device Development in Monocrystalline Diamond Films," Quarterly Report, June 30, 1991).

II. Interface Reactions of Titanium on Single Crystal and Thin Film Diamond Analyzed by UV Photoemission Spectroscopy

J. VanderWeide and R.J. Nemanich

Department of Physics, North Carolina State University,
Raleigh, NC 27695-8202, USA

Abstract

The reactions of titanium on natural crystals and CVD polycrystalline thin films were studied by uv-photoemission spectroscopy. The focus of this study was to characterize the interface reactions and to determine the Schottky barrier of titanium on diamond, deposited and annealed in UHV. Spectroscopic features attributed to the electronic states of Ti-C were identified, and the formation of titanium carbide was observed as a function of annealing temperature. The onset of a titanium-carbon reaction was observed after the 400°C anneal. A well defined TiC spectra was observed after annealing to 600°C. The Schottky barrier height from Ti on natural p-type diamond (111) was obtained by determining the valence band maximum and the Fermi level, and a barrier height of 1.0±0.2 eV was found.

Introduction

Along with the rapidly advancing field of CVD diamond thin films for electronic applications, there is an increased interest in metal contacts on diamond. These contacts can be either ohmic or rectifying, depending on the metal, surface preparation prior to metal deposition and treatment of the contact [1]. Titanium is known to form a Schottky contact on diamond when deposited at low temperatures but is generally used to form an ohmic contact by annealing the contact above 580°C [2,3], or by depositing the titanium while the diamond is kept at 400°C [4]. The transition from rectifying behavior to ohmic behavior after annealing has been shown for carbide forming metals [2]. In this study we have employed angle resolved uv-photoemission spectroscopy, (ARUPS), to observed the onset of titanium carbide formation for UHV deposited titanium films on both single crystal diamond and diamond thin film.

Although there have been many reports of the rectifying behavior of titanium on diamond, to our knowledge no measurements of the Schottky barrier height have been reported. Due to the high ideality factor of the titanium-diamond rectifying contact it is generally difficult to determine the Schottky barrier height using I-V measurements. The position of the valence band maximum on the surface of diamond relative to the Fermi level of a titanium film can be determined from the ARUPS data. The energy difference is the Schottky barrier height for the metal on a p-type semiconductor. This technique was used to determine the Schottky barrier height for UHV

deposited titanium on both diamond thin film and single crystal, type IIB, diamond with a (111) orientation.

Experimental

The ARUPS data was measured with a 50mm hemispherical analyzer with an ultimate energy resolution of 0.02eV and an angular resolution of 2°. The analyzer is mounted on a two stage goniometer which allows angle dependent measurements. As an excitation source a differentially pumped helium discharge lamp was used, which generated HeI (21.2eV) radiation. The base pressure of the ARUPS chamber was $<1 \times 10^{-9}$ Torr with an operating pressure of 5×10^{-9} Torr. The sample was mounted on a heating stage which allows the samples to be annealed up to ~1000°C. The ARUPS chamber is equipped with a Ti-filament deposition source. The pressure during deposition was $\sim 5 \times 10^{-8}$ Torr which dropped rapidly after the filament was turned off. The samples can be transferred from the ARUPS chamber under UHV conditions into a rf-plasma chamber. Both argon and hydrogen plasmas were employed to clean the diamond surfaces.

The single crystal diamond wafers, 3x3x0.5 mm, type IIB, with (111) orientation, were polished in 0.25 μm diamond grid and chemically cleaned prior to loading into the vacuum. The chemical cleaning procedure consisted of a 10 min. etch in fuming sulfuric acid, to remove wax used to hold the diamond in the polishing process, a 45 min. etch in fuming chromic acid, to remove graphitic material and concluded by a 10 min. etch in aqua regia to remove metal contaminants. The chromic acid was produced by saturating sulfuric acid with CrO_3. Once in vacuum the sample was further cleaned in a H and Ar plasma before Ti was deposited. The diamond thin films used in this study were grown in a hot filament system. These samples were loaded into the vacuum without *ex situ* cleaning. The samples were however annealed *in situ* to above 750°C for 10 min. and exposed to an H/Ar plasma for 30 min. prior to Ti deposition. All the samples were mounted with Ta wire on a Molybdenum sample holder. Spectra were obtained for increasing titanium coverages until the diamond features in the spectrum were totally replaced by Ti features. For the annealing study a 30Å layer of Ti was deposited and consequently annealed at increasing temperatures in 100°C increments, for 5 min., after which spectra were obtained.

Results and Discussion

In order to determine the Schottky barrier height from ARUPS data, it is necessary to determine the position of the valence band edge in the spectra. The uv-photoemission spectrum of single crystal diamond C(111) at surface normal emission is shown in Fig. 1. The valence band edge can be clearly distinguished by the onset of emission at about 1 eV below the Fermi level. The valence band edge position was determined by linear extrapolation of the slope to zero and was found to be 8.1 eV above the strong peak near 8.5 eV. The valence band position was expressed relative to this peak since it remained visible for increasing titanium coverages. In the same figure a spectrum is shown of the C(111) surface at an angle of 30° off normal along the [110] direction. in this spectrum, the onset of emission shifted -0.6 eV while the strong peak shifted +0.3 eV, the difference between the onset of emission and the reference peak is found to be 7.2 eV. We suggest that the differences in the onset are caused by a downward dispersion of the valence band edge

away from the Γ point in the bandstructure [5]. The spectrum at surface normal emission reflects the valence band at the Γ point and shows therefore the valence band maximum. A spectrum of a diamond thin film is shown in Fig. 1. For the film, the onset of the emission appears at 7.5 eV above the main peak. We suggest that this is due to the fact that the diamond thin film consists of randomly oriented crystals, which makes the spectrum of diamond thin films in effect equivalent to an angle integrated spectrum of single crystalline diamond. The relative energy of the valence band to the strongest feature of the ARUPS for single crystal diamond at normal emission angle was therefore used to determine the valence band maximum. The determination of the valence band maximum and hence the Schottky barrier height is less accurate however, since the position of the main peak is also angle dependent, as noted above.

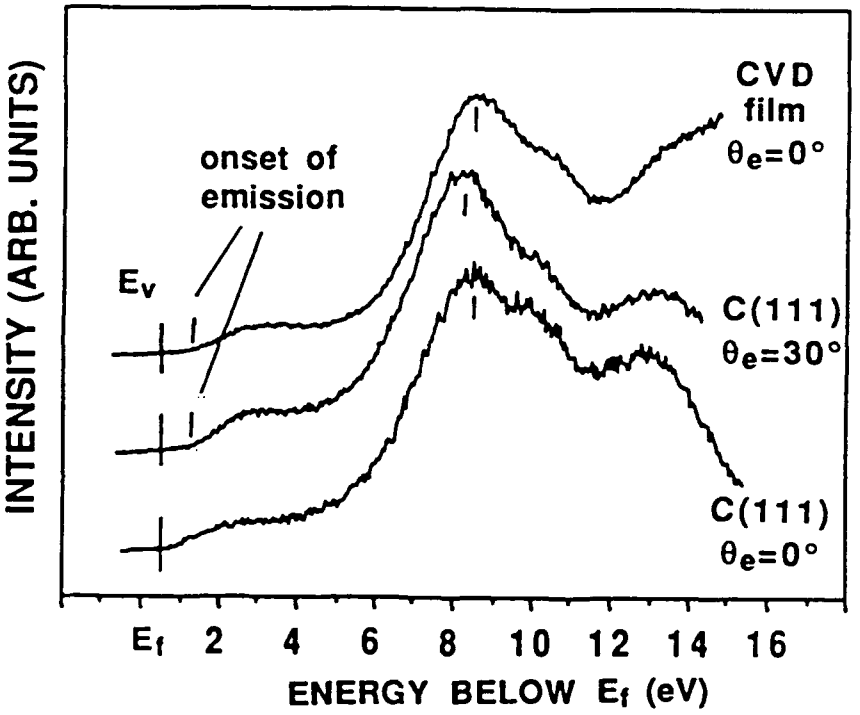

Fig. 1 ARUPS spectra of C(111) at normal emission and at 30° off normal, along the 110 direction and of diamond thin film. The solid line shows the position of the valence band maximum, derived from the onset of the C(111) spectrum at surface normal. The vertical lines show the onset of the of the other spectra.

In order to determine the Schottky barrier height, titanium was deposited at room temperature on the single crystal diamond (Fig. 2) and the diamond thin film (Fig. 3). After the first deposition of titanium on the C(111) surface no titanium features could be discerned although the spectrum shifted by 0.45 eV toward lower energies. After further deposition a sharp Fermi edge developed, due to emission from the d-band of titanium. The diamond

valence band energy was determined using the method described above, and a barrier height of 1.0±0.2 eV was deduced. Following the first deposition of <1Å of titanium on the diamond thin film, no titanium could be detected in the ARUPS spectrum, and the spectrum was found to shift 0.35 eV toward lower energies. After further titanium deposition the Fermi level developed while the diamond features were attenuated but still visible. Again, from these spectra, the diamond valence band maximum was determined, and a Schottky barrier height of 0.9 (+0.5/-0.2) eV was found for titanium on the diamond thin film. The asymmetry in the error is related to the fact that the main peak position is angle dependent.

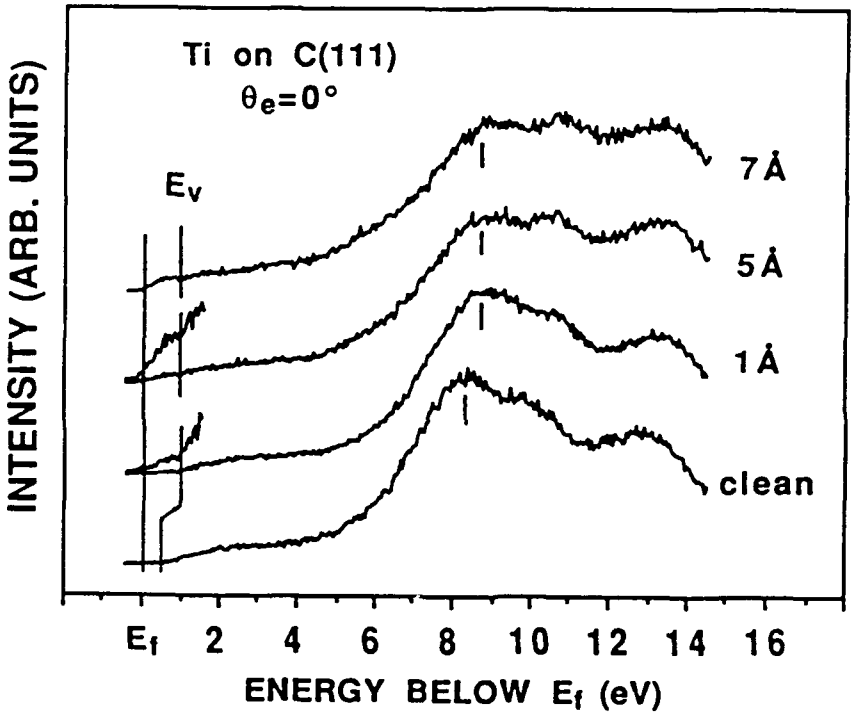

Fig. 2 Normal emission spectra of C(111) as a function of titanium coverage.

ARUPS spectra of the annealing of a 30Å layer of titanium on a diamond thin film are shown in Fig. 4. The emission at the Fermi edge is again due to the titanium d-band. It has been suggested that the broad peak near -5.5 eV is due to a contamination of the deposited titanium layer, possibly oxygen or hydrogen [6]. No diamond features could be discerned. Subsequent spectra were obtained after annealing the film at increasing temperatures, at 100°C increments. After annealing the film to 400°C a peak starts to appear around -3.5eV and gets more pronounced after annealing to higher temperatures for 5 minutes at a time. This peak is associated with Ti-C bonding [6] and shows the development of Ti-carbide formation which reaches its completion after a 600°C anneal. This correlates well with the transition from rectifying behavior to ohmic behavior as described by Gildenblat [3].

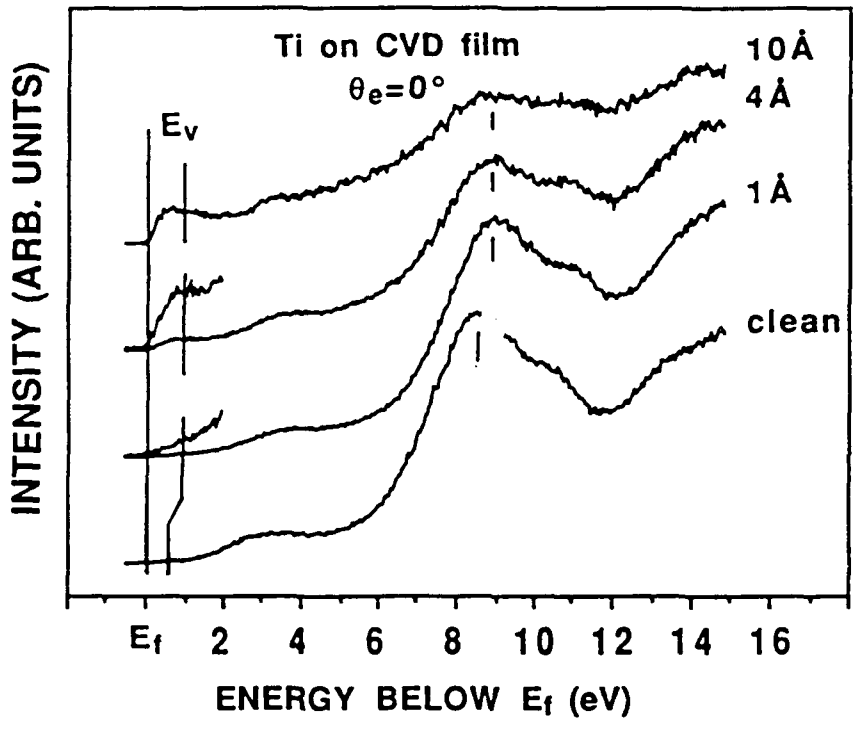

Fig. 3 Normal emission spectra of diamond thin film as a function of titanium coverage.

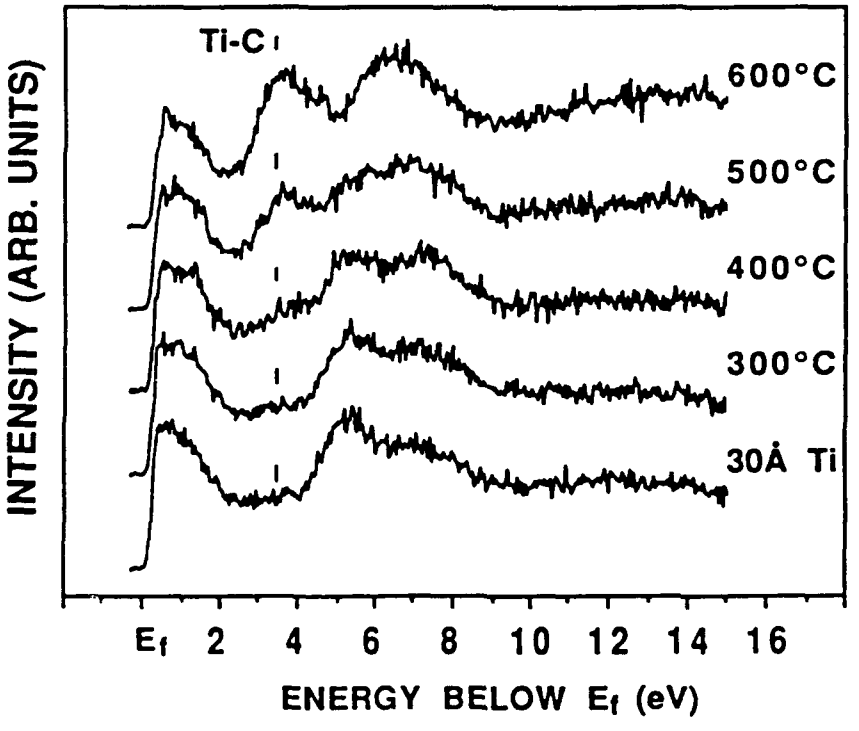

Fig. 4 Normal emission spectra of diamond thin film with 30Å Ti as a function of annealing temperature. The peak appearing at 3.5 eV below the Fermi level is indicative of Ti-C formation.

Summary

Using ARUPS the Schottky barrier height was determined for titanium on both single crystal diamond and diamond thin film. The Schottky barrier height of titanium on single crystal diamond was found to be 1.0±0.2 eV which compared well with the value of 0.9 (+0.5/-0.2) eV found for titanium on diamond thin film. Also the transition from titanium to titanium-carbide was observed to occur for a 30Å layer of Ti on diamond thin film after a 600°C anneal. The onset of the interface reactions were observed at 400°C.

Acknowledgements

We thank K. Das of Kobe Research for his help in establishing a cleaning procedure for the diamond wafers, T. Schneider for the plasma cleaning work and T. Humphreys for helpful discussions. We also acknowledge F. Jansen and M.A. Machonkin of Xerox Corp. for suppling the diamond thin films. This study was supported in part by the Office of Naval Research (Contract #N00014-90-J-1707) and the MITI of Japan through the NEDO program.

References

[1] Y. Mori, H.i Kawarada, A. Hiraki, Appl. Phys. Lett **58**, 940 (1991)
[2] K.L. Moazed, R. Nguyen, J.R. Zeidler, IEEE Electr. Dev. Lett. **9**, 350 (1988)
[3] G. Sh. Gildenblat, S. A. Grot, C. W. Hatfield, A.R. Badzian, T. Badzian, IEEE Electr. Dev. Lett. **11**, 371 (1990)
[4] H. Shiomi, H. Nakahata, T. Imai, Y. Nishibayashi, N. Fujimori, Jap. J. of Appl. Phys., Part 1 (Regular Papers & Short Notes) **28**, 758 (1989)
[5] G.S. Painter, D.E. Ellis, A.R. Lubinsky, Phys. Rev. B **4**, 3610 (1971)
[6] D.E. Eastman, Solid State Comm. **10**, 933 (1972)

III. TITANIUM-BASED COMPOUNDS AS ELECTRICAL CONTACTS FOR DIAMOND (J. T. Kelliher and K. J. Bachmann)

The objective of this program is to explore the utility of deposited contacts to diamond. The deposition of TiN avoids chemical interactions of the contact metal and the underlying diamond. This will alter the defect chemistry under the contact relative to that of the pure metal contact and thereby affect the electrical properties.

We have chosen remote plasma-enhanced chemical vapor deposition (RPCVD) and plasma-assisted chemical beam deposition (PACBD) as processing methods, since low temperature deposition and high resolution are generally desirable aspects of the contact formation process. The work on engineered interlayers in the context of contacts to diamond supplements the work of Tachibana in the laboratory of Professor Glass and VanderWeide in the laboratory of Professor Nemanich who have studied the formation of Au, Al and Ti contacts to diamond including the reactive formation of titanium carbide upon annealing of Ti metal films directly deposited onto diamond.

In order to carry out the proposed research, a RPCVD/PACBD system has been designed and built. The system operates in the RPCVD mode in the milli-torr range and in the PACBD mode in the 10^{-7} to 10^{-5} torr range. System overviews for operation in these two modes are presented in Figures 1 and 2. The load lock and substrate heating stage presently permit the use of wafers with diameters to 2", but they can be upgraded to wafer dimensions ≤6" if required. The ECR source shown in Figure 2 replaces the rf plasma source shown in Fig. 1 under the conditions of PACBD. The former source is presently not part of the system and will be added in the future.

Initial runs with the system have employed the RPCVD process for TiN deposition. Presently Si substrates are being used to determine the correct processing parameters (optimum deposition temperature, gas flow rates, plasma power, etc.). The initial results using $TiCl_4$ and N_2 introduced through the dispersal rings with H^+ enhancement of the deposition rate allow the deposition of TiN_x at temperatures between 400-500°C. Selective deposition has also been achieved. The TiN_x deposits readily on the bare silicon, but no deposition of TiN occurs on SiO_2 covered regions. At present, the films are Ti-rich; thus, must be made in the processing parameters to deposit stoichiometric TiN. These adjustments are presently being established. Also, the introduction of the N_2 into the plasma region and the alternative use of NH_3 instead of N_2 will be evaluated.

Future research will include the use of the PACBD technique in order to achieve higher resolution in both the lateral contact dimensions and layer thickness. These parameters will be important in the implementation of miniaturized devices on polycrystalline diamond films and multilayer contacts.

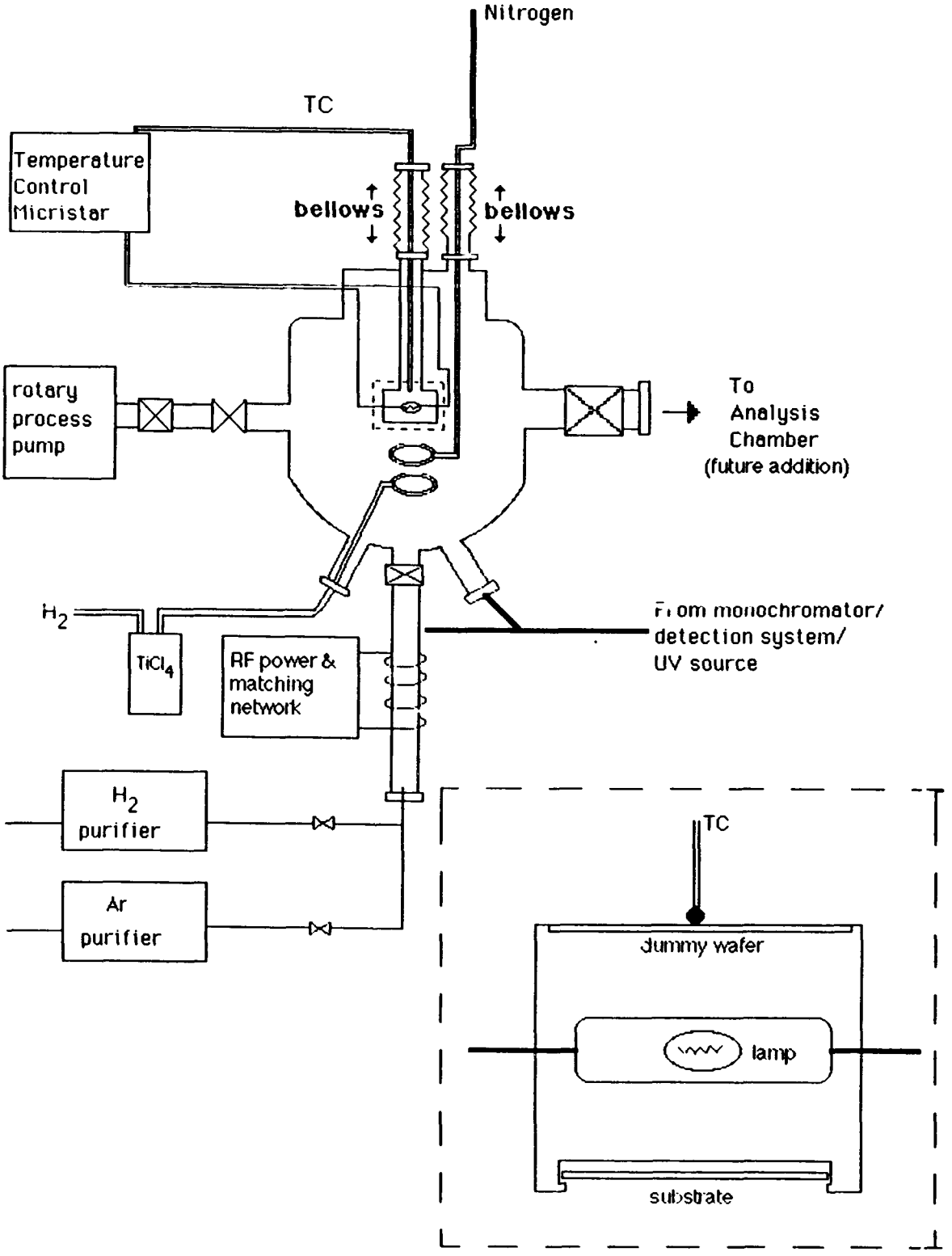

Figure 1. Remote plasma chemical vapor deposition.

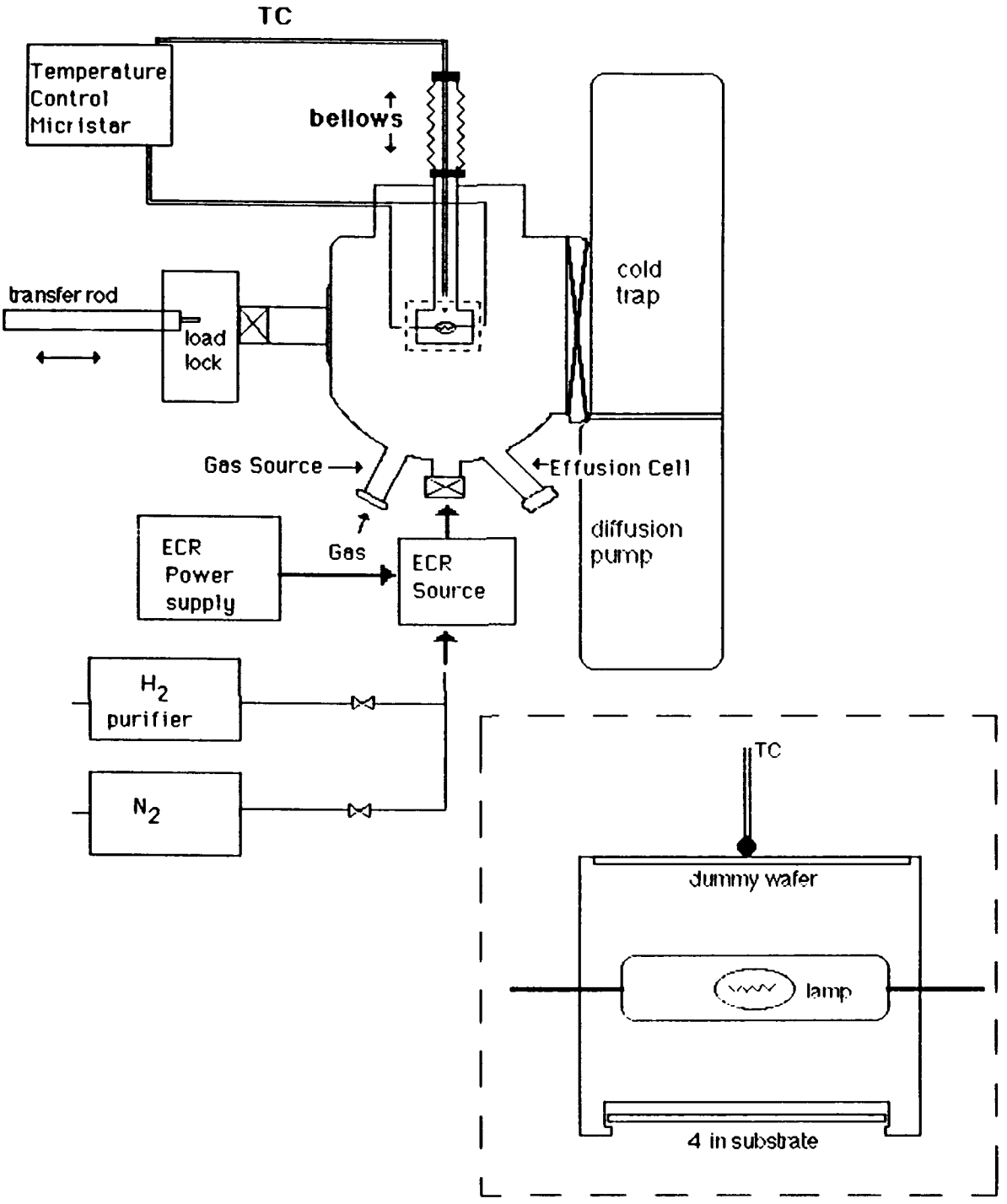

Figure 2. Chemical beam deposition.

IV. ELECTRICAL CONDUCTIVITY OF DIAMOND FILMS FROM ROOM TEMPERATURE TO 1200C

S.F. Adams[a], J.W. Vandersande[b], D. Zolton[b],
B.R. Stoner[c], and J.A. von Windheim[c]

[a]Wright Laboratory/POOC
Wright Patterson AFB, OH 45433

[b]Jet Propulsion Laboratory
California Institute of Technology
Pasadena, CA 91109

[c]Materials Research Center
North Carolina State University
Raleigh, NC 27695

ABSTRACT

Diamond films have the potential of being used as the high temperature insulator in space nuclear power components such as thermionic and thermoelectric energy conversion devices. The bulk electrical resistivity of the films should be sufficiently high and the films should be stable at the highest operating temperatures of these components. There appears to be a large difference (several orders of magnitude) in room temperature resistivity between films fabricated using various techniques, conditions, and substrates. A variation in resistivity between films at high temperatures has also been observed but is not as pronounced as at room temperature. The resistivities of several films have been measured from room temperature to 1200C and will be reported. The Raman Spectra of the films were taken and they were examined in the SEM. The resistivities have also been compared to that for natural type IIa diamond.

INTRODUCTION

The energy conversion components of high temperature space nuclear power sources (thermionic and thermoelectric) have the need for a high temperature electrical insulator that is structurally and electrically stable under the continuous exposure to the harsh environment of a space nuclear reactor. The insulator would need to maintain exposure to at least a temperature of 800C, a 1 MeV neutron fluence of 10^{22}n/cm^2, and possibly direct contact with a liquid alkali metal coolant. The ideal material for this application would maintain a high bulk electrical resistivity to prevent leakage current losses while providing a high thermal conductivity to enhance the cooling process of

Presented at: 2nd Int. Symp. on Diamond and Diamond Materials, ECS Meeting, Washington, DC, May 5-10, 1991. To be published: ECS Symposium Series.

certain components. A diamond film is an excellent candidate to be this insulator if it can fulfill these requirements.

The diamond films that appear to have the most promise of meeting these requirements are those synthesized by plasma-enhanced chemical vapor deposition (PECVD) techniques. These films display typical Raman spectra of diamond with a strong, sharp diamond bonded carbon signal at 1332 wave numbers and, for some films, a lesser and more broad non-diamond bonding signal at 1550 wave numbers representing a graphitic or amorphous carbon component. A comparison of the electrical properties of these films with those of natural diamond over a wide range of temperature is a good indicator of the high temperature insulating performance of state-of-the-art diamond films.

The thermal conductivity of PECVD diamond films at room temperature has been measured to be around 18 W/cm-K [1] indicating that these diamond films are superior in this property to all known materials at room temperature except for natural diamond (20 W/cm-K for type IIa). The electrical resistivity of many diamond and diamond-like films have been measured at room temperature. Resistivity values at this temperature have ranged anywhere from 10^6 - 10^{14} ohm-cm compared to 10^{16} ohm-cm for natural type IIa (low nitrogen content) diamond. From this prior data, it appears that diamond films deposited to date have not equaled the electrical insulating properties of natural diamond at room temperature. There is a lack of data, though, for diamond films and natural diamond resistivity at high temperatures (above 700C).

We recently presented results which were the first electrical conductivity/resistivity measurements of diamond and diamond film at temperatures up to 1200C [2]. Two natural IIa diamonds, two diamond films, and three diamond-like films were evaluated in this study. The diamond films displayed high temperature resistivities that, in one case, approached that of the natural diamond and, in the other, actually exceeded the resistivity of the natural diamond. An activation energy of 1.4 eV was found for both of the natural diamonds from the slope between 300 and 1200C. The diamond films appeared to have different conduction mechanisms between the temperature ranges of 200 to 600C and 600 to 1200C with activation energies of 0.9 eV and 1.8 eV respectively.

It is clear from a review of previous studies that the processing techniques of the diamond films has a substantial effect on the electrical quality of the sample. As the deposition of diamond film is becoming a popular among many researchers, the importance of utilizing well established sources of test samples is emphasized.

Measuring the electrical resistivity of diamond films to higher temperatures and then back down to room temperature will also provide information regarding the stability of the films and the bonding of the film to the substrate. There is also evidence that

post-growth heat treatment of diamond films stabilizes the electrical activity of the hydrogen within the film which increases the bulk electrical resistivity [3]. This behavior can be verified by the resistivity measurements during thermal cycling.

EXPERIMENTAL

An apparatus was specifically designed and built with the ability to measure very high resistivity insulators up to a temperature of 1. 00C. The sample holder and oven are shown in Figure 1. The holder was made of 998 pure alumina and all of the wiring feedthroughs and connections were made in such a way to ensure that leakage currents bypassing the sample were as low as possible. A DC two probe method with a guard ring and volume guard were used to measure the bulk electrical resistivity of the samples perpendicular through the plane of the samples. A long niobium center probe rested, with some pressure, on a small iridium disk on top of the sample. A cylindrical niobium volume guard fit around the center probe and also rested on the top of the sample. A large area iridium electrode was placed underneath the sample as the second probe.

The conductivity measurement limits of the apparatus has been characterized and the results presented [2]. Below 900C, a slight conductivities of 10^{-16} to 10^{-17} $ohm^{-1}cm^{-1}$ were measured using a highly resistive sapphire sample. It is believed that lower conductivities cannot be measured (i.e. a maximum resistivity of 10^{16} to 10^{17} ohm-cm).

The diamond films used in this study were two samples from Crystallume, two samples from North Carolina State University, and one sample from a joint research effort by Wright Laboratory and Universal Energy Systems (UES). A natural type IIa diamond was also evaluated and considered in the results. One diamond film from Crystallume, sample CSW-M-6-NS, was deposited on a silicon substrate by a microwave assisted PECVD method. The film thickness was calculated by Crystallume, based on nominal growth rates, to be 6 microns. The other film from Crystallume, sample 7-B-171 was a 3 micron diamond film deposited on a molybdenum substrate using DC plasma-enhanced CVD techniques. The molybdenum substrate represents a refractory metal material that will likely be used in thermionic or thermoelectric energy conversion components. The DC deposition technique would also likely be used in fabricating a thermionic diamond sheath insulator. Both of these samples were post-growth heat treated at Crystallume's facility.

Both samples from North Carolina State University were grown in Astex cylindrically coupled stainless steel microwave plasma CVD reactor. The first film, sample BS13-B2, was grown immersed and the second sample, BS3-A, was grown down stream from the plasma. Both films were grown on undoped silicon (100) substrates with a methane-to-hydrogen ratio of 1%. Neither film received any post deposition treatment. Samples BS13-B2 and BS3-A were approximately 9 microns and 5.5 microns thick

HIGH TEMPERATURE INSULATOR
ELECTRICAL RESISTIVITY MEASUREMENT STATION
SAMPLE HOLDER AND OVEN

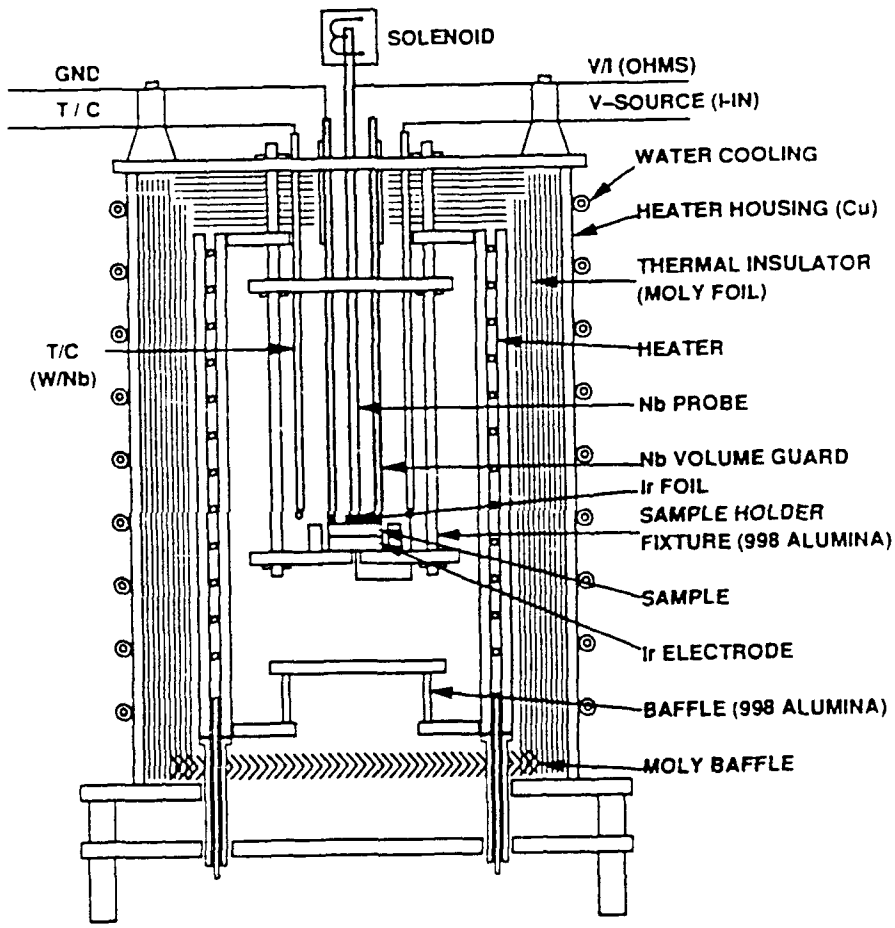

Figure 1

respectively, as determined from cross-sectional SEM.

The UES/ Wright Laboratory sample was a 5 micron thick film deposited on a silicon substrate using a microwave assisted PECVD technique. The deposition process was still being optimized for high resistivity films at the time that this sample was submitted. This sample was, therefore, considered to represent a slightly less than state-of-the-art quality insulating diamond film.

EXPERIMENTAL RESULTS AND DISCUSSION

The electrical conductivity measurements of the two diamond film samples from Crystallume compared with a type IIa natural diamond are shown in Figure 2. The room temperature resistivities of both samples were extremely high, with the diamond film on molybdenum, sample 7-B-171, approaching natural diamond at the maximum measurement limit (just below 10^{16} ohm-cm). At a temperature of 1000K, the resistivities of both films were approximately equal at 5 x 10^5 ohm-cm, while the natural diamond remained slightly higher at 10^6 ohm-cm. The activation energies, determined from the slope between 40°C and 300°C, of CSW-M-6-NC and 7-B-171 were 0.6 eV and 0.9 eV respectively. A different conduction mechanism between 300°C and 800°C was most likely responsible for higher activation energies of 0.9 eV and 1.1 eV for the respective films. These higher values can be compared to the natural diamond activation energy of 1.4 eV in that temperature range [2].

The electrical conductivity measurements of the UES/ Wright Laboratory diamond film are shown in Figure 3. The sample had a room temperature resistivity of approximately 10^{13} ohm-cm but the resistivity at 1000K was measured to be slightly higher than that of natural diamond. The conduction mechanisms of this film can be characterized by activation energies of 0.1 eV between 40°C and 300°C and 0.8 eV between 300°C and 900°C.

The electrical conductivity measurements of the North Carolina State University diamond films are shown in Figure 4 and 5. The most outstanding features of these two plots are the initial room temperature resistivity measurements. The resistivity values are several orders of magnitude less than the eventual room temperature resistivity once the films had undergone at least one temperature cycle. Since these films were not post-growth heat treated, this observation agrees with earlier results [3], where it was theorized that electrical activity of hydrogen in the film is responsible for the excess electrical conduction at room temperature. The resistivities at 1000K for both films were between 10^5 and 10^6 ohm-cm. Both films displayed activation energies of 0.8 eV at temperatures above 300°C.

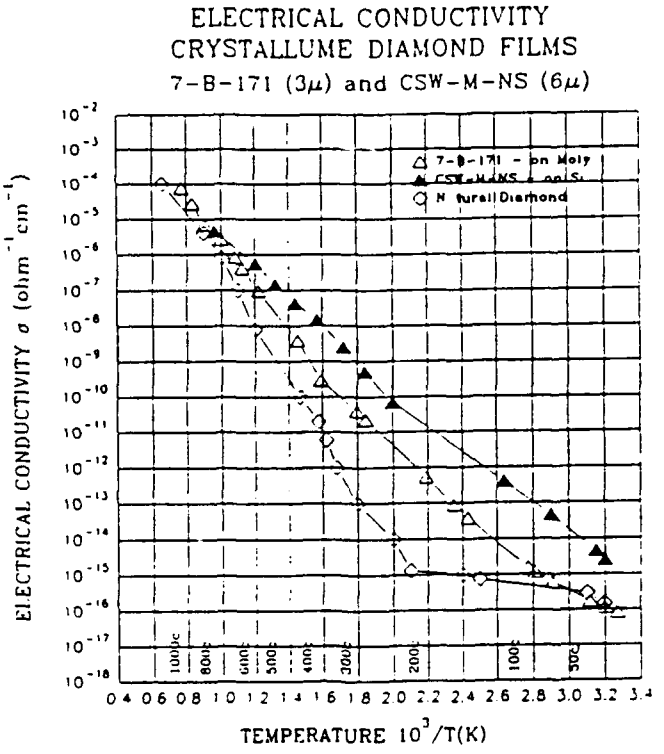

Figure 2

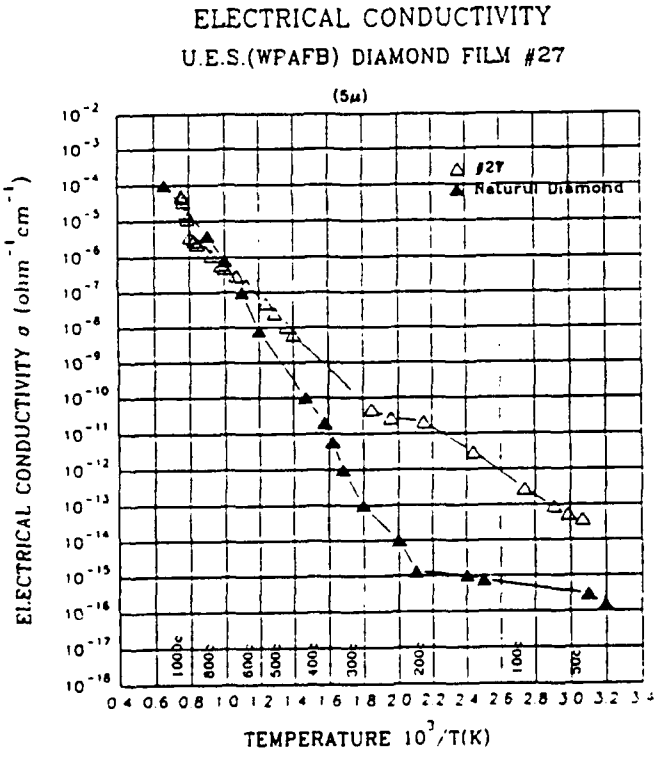

Figure 3

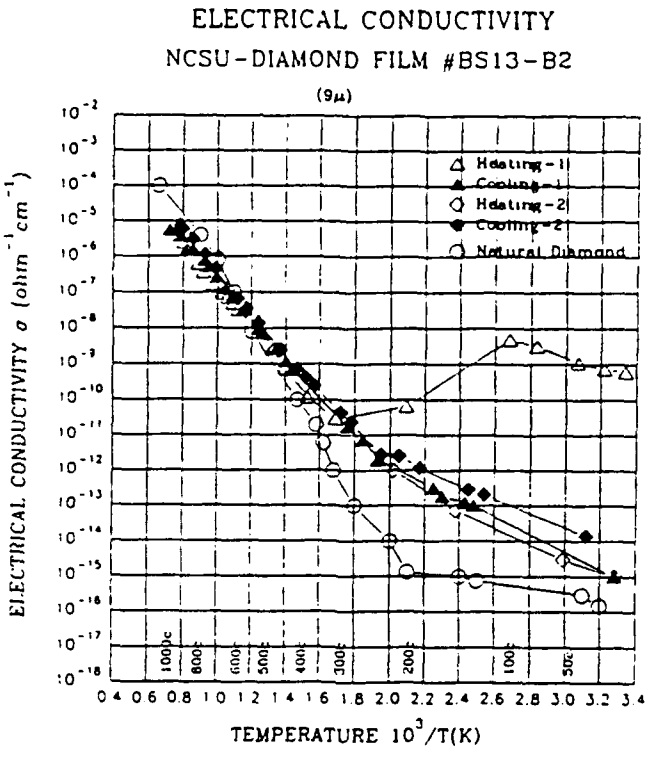

Figure 4

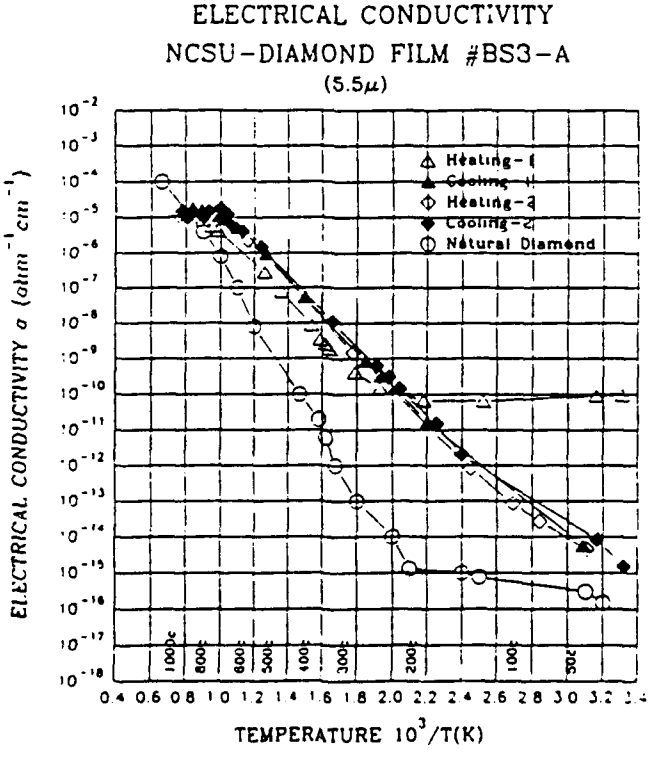

Figure 5

SUMMARY

The electrical conductivity of five diamond films from three different sources were measured from room temperature to 1200°C. The room temperature electrical resistivities of the different films varied several orders of magnitude depending on the processing techniques used during deposition. One of the Crystallume samples was measured to have a room temperature resistivity which is the highest measured to date, but still below the "actual" value for natural diamond. The initial room temperature resistivities of both of the North Carolina State University diamond films were very low due to the absence of post-growth heat treatment in the processing of these samples.

The electrical conductivity values converged at higher temperatures and there was much less variation between films at a temperature of 1000K. The natural diamond and all of the diamond films had measured resistivities between 10^5 and 2 x 10^6 ohm-cm at 1000K. This is of much interest since a diamond film would most likely be maintained around this temperature in a space nuclear power component application. Systems studies must be completed to realize if these electrical properties at 1000K are adequate for each thermionic or thermoelectric application.

The activation energies of the five diamond films ranged from 0.1 eV to 1.1 eV compared to 1.4 eV for the natural diamond. This range of activation energies shows how different processing techniques can lead to a variation in impurity characteristics and conduction properties. It is suggested that vacancy loops or acceptor/donor impurities at the grain boundaries of the diamond films are responsible for the various conduction mechanisms and resulting activation energies. Considerably more work needs to be done to get a better understanding of the fundamentals of the conduction mechanisms.

Research supported by SDIO/IST & managed by Wright Laboratory

1. J.A. Herb, C. Bailey, K.V. Ravi, and P.A. Dennig, "The Impact of Deposition Parameters on the Thermal Conductivity of CVD Diamond Films", Proceedings of The First International Symposium on Diamond and Diamond-Like Films, Proc. Vol. 89-12, The Electrochemical Society, Los Angeles (1989), p366.

2. J.W. Vandersande and L.D. Zolton, "High Temperature Electrical Conductivity Measurements of Natural Diamond and Diamond Films", To be published in "Surface and Coatings Technology", Proceedings of the First European Conference on Diamond and Diamond-Like Carbon Coatings, Sept 17-19, 1990.

3. M.I. I andstrass and K.V. Ravi, "The Resistivity of CVD Diamond Films", Appl. Phys. Lett. 55, 1391 (1989).

The Potential of Diamond and SiC Electronic Devices for Microwave and Millimeter-Wave Power Applications

ROBERT J. TREW, FELLOW, IEEE, JING-BANG YAN, MEMBER, IEEE, AND PHILIP M. MOCK, MEMBER, IEEE

Invited Paper

There is significant interest in developing microelectronic devices for blue emission, high temperature, high power, high frequency, and radiation hard applications. This interest has generated significant research effort in wide bandgap semiconductor material, in particular SiC and semiconducting diamond. Both of these materials are similar in crystal structure with half of the carbon atoms in the diamond structure replaced by Si to produce SiC. However, the latter material exists in a host of polytypes, the causes of which are not completely understood. The deposition of monocrystalline diamond at or below 1 atm total pressure at $T<1000°C$ has been achieved on diamond substrates, although deposited film has been polycrystalline on all other substrates. For significant application to electronic devices, the heteroepitaxy of single crystal films of diamond and an understanding of mechanisms of nucleation and growth, methods of impurity introduction and activation, and further device development must be achieved. The technology of producing SiC is more advanced and the deposition of thin films and the associated technologies of impurity incorporation, etching, and electrical contacts have culminated in a host of solid-state devices. In this paper, the potential of SiC and diamond for producing microwave and millimeter-wave electronic devices is reviewed. Both of these materials have been proposed for fabrication of devices capable of producing RF output power significantly greater than can be achieved with comparable devices fabricated from commonly used semiconductors such as Si and GaAs. Theoretical calculations are presented of the RF performance potential of several candidate high frequency device structures: the MEtal Semiconductor Field-Effect Transistor (MESFET), the IMPact Avalanche Transit-Time (IMPATT) diode, and the Bipolar Junction Transistor (BJT).

I. INTRODUCTION

The utilization of semiconducting SiC and diamond for high frequency electronic devices has been of interest to device physicists for many years. For example, the electronic properties of diamond were investigated in the 1930's [1] and serious work with SiC dates at least to the early 1960's. Some of the initial interest in these materials was for high temperature, corrosion resistant semiconductors. As the material parameters became better known it became apparent that these materials possess a combination of parameters that, in many respects, make them ideal for various applications, including high frequency devices. Diamond has been proposed for use as detectors (radiation and ultraviolet photodetectors), power and microwave devices (bipolar, field-effect, and permeable base transistors, IMPATT diodes), green-blue LED's, thermistors, and switching devices. Devices that can be fabricated from SiC include LED's, thermistors, MESFET's, bipolar and heterojunction transistors, and various types of diodes.

The early attempts to utilize these materials were hindered by technological problems related to crystal growth and purity and to the development of suitable ohmic and rectifying contacts. Although rapid progress has been made in recent years on solutions to these problems, growth and device fabrication technology is still primitive compared to Si and GaAs and the necessary technology has not yet developed to the point where high performance devices can be easily fabricated. At the current state-of-the-art, SiC technology is more advanced than that for diamond and electronic devices are being reported. Preliminary work has also been reported on diamond devices using both natural and synthetic crystals.

In this paper, the potential of SiC and diamond for producing high performance microwave and millimeter-wave electronic devices is investigated. It is shown that both of these materials possess characteristics that may permit RF electronic devices with performance similar to or greater than what is available from devices fabricated from the conventional semiconductors, Si, GaAs, and InP.

Manuscript received October 25, 1990; revised January 14, 1991. This work was supported by the SDIO/ONR under Contracts N00014-86K-0666, N00014-90-J-1604, and N00014-88-K0341.

The authors are with the Electrical and Computer Engineering Department, North Carolina State University, Raleigh, NC 27695-7911.

0018-9219/91/0500-0598$01.00 © 1991 IEEE

The investigation makes use of theoretical computer simulations of the MEtal Semiconductor Field-Effect Transistor (MESFET) and the IMPact Avalanche Transit-Time (IMPATT) diode. Bipolar Junction Transistor (BJT) operation is also investigated by means of a large signal microwave equivalent circuit model. These devices represent some of the most commonly used electronic devices for microwave and millimeter-wave applications and also, the most likely devices to be suitable for fabrication from the wide bandgap semiconductors. Of these, the MESFET is of particular interest since it is structurally a simple device and readily fabricated in a variety of semiconductor materials. The MESFET can be operated over a wide frequency range extending from the low megahertz (MHz) region to well into the millimeter-wave bands (i.e., well over 100 GHz). The IMPATT diode can also have a relatively simple structure and is attractive for high frequency applications. IMPATT devices fabricated from GaAs and Si have operated as high as 250 GHz and 430 GHz, respectively. The BJT has a relatively complex structure and high performance devices will most likely be difficult to fabricate in wide bandgap semiconductors. In particular, technological and material problems will likely limit the high frequency performance of these devices to the low microwave region. However, BJT's fabricated from wide bandgap semiconductors are attractive candidates for low frequency (UHF and below) power applications.

The accuracy of the theoretical calculations is dependent upon the values used for the material parameters required in the device models. For extensively used semiconductors such as Si and GaAs, these parameters have been studied using a variety of experimental and theoretical techniques. For SiC and especially for diamond, however, the material parameters are not well known. Semiconducting diamond has not yet been well characterized due to significant difficulties in producing device quality material. Suitable techniques for introducing donor impurities with reasonable activation properties to create n-type semiconducting layers in diamond are not currently known. Boron can be introduced into diamond to produce p-type epitaxial layers. However, the relatively high activation energy of boron acceptors may require high temperature operation (e.g., 500°C–600°C) to obtain appropriate charge densities. Since hole transport rapidly degrades with temperature, demonstrating approximately a $T^{-2.8}$ temperature sensitivity, it may prove difficult to fabricate high performance p-type microwave devices.

The material data used in this work was obtained from published reports and from discussions with various researchers. Although uncertainty exists in specific parameter values an attempt was made to select reasonable values for use in device applications. The diamond device calculations assume the existence of activated n-type semiconducting epitaxial layers. Although such crystals do not presently exist, the available data indicates that n-type material would produce the highest performance devices. Future research may result in the availability of suitable device quality material.

II. Background

A. SiC

Silicon carbide is the only compound in the SiC system that exists in the solid state, but it can occur in many polytype structures [2], [3]. More than 170 polytypes have been identified. The lone cubic polytype crystallizes in the zincblende structure and is denoted as 3C- or β-SiC. The additional hexagonal (H) and rhombohedral (R) polytypes are collectively referred to as α-SiC. The most common polytypes are 3C and 6H; however, 4H, 15R, and 2H have also been identified in crystalline form, but are rare. Most of the polytypes are extremely stable, except that 2H is unstable and can transform to other polytypes at temperatures as low as 400°C. The most stable polytype is 6H-SiC [4].

Silicon carbide does not exist in significant quantities in nature. The first reported synthesis was accidental: the result of attempts by Berzelius to make diamond. The development of the Acheson process [5] in 1891 brought SiC production to commercial scale in the abrasives industry. Initial SiC research was generally conducted using crystals that were occasional by-products of this process. In 1955, Lely [6] developed a laboratory version of the industrial sublimation process and was able to produce rather pure α-SiC single crystals. Due to the growth temperature of about 2500°C, only α-SiC polytypes were produced in the Lely process. Growth of β-SiC was sometimes observed during the cool down phase. The doping level of the SiC crystals depends strongly upon the impurity content of the starting material, the quality of the argon atmosphere, as well as temperature and duration of degassing cycles used in this process. The success of the Lely process led to significant research effort directed toward development of SiC during the 1960's.

The electron transport characteristics of β-SiC over the temperature range of 27°C–730°C are predicted from theoretical calculations to be significantly greater than can be obtained from α-SiC due to reduced phonon scattering in the cubic material. For this reason, there is significant interest in the growth of thin films of β-SiC for device applications. Epitaxial films of β-SiC have primarily been grown on chemically converted surfaces of monocrystalline Si(100) substrates by chemical vapor deposition using the high purity gases of SiH_4 entrained in the carrier gas of H_2. A review of growth techniques can be found in [7], [8]. Silicon carbide can be doped n- or p-type by diffusion [9], epitaxial growth [10], [11], and ion-implantation [12]–[14]. The diffusion of dopants into SiC requires temperatures around 1900°C, and special precautions are necessary to prevent sublimation of the bulk crystal at this temperature. Moreover, this temperature is considerably above the melting point of SiO_2, and no commercially attractive alternative diffusion masking material has yet been found. Therefore, doping during epitaxial growth or ion implantation with B or Al (p-type) and P or N (n-type) is more suitable for SiC devices. Using epitaxial growth, the dopant gases of N_2 (or NH_3),

PH_3, B_2H_6, and $AlCl_3$ (or $Al(CH_3)_3$ carried in H_2) are incorporated directly into the primary gas stream during chemical vapor deposition. For ion implanted crystals, damaged or amorphous regions are annealed at a temperature between 1400°C and 1800°C [14]. Unintentionally doped β-SiC epilayers are usually n-type with electron concentrations and mobilities of 3×10^{16}–3×10^{17} cm^{-3} and 250–550 cm^2/V-s, respectively [15].

Historically, SiC can be considered one of the first known semiconductors and electroluminescence was reported by Round [16] in 1907. Blue light-emitting diodes (LED's) have been fabricated by epitaxial deposition of SiC from carbon-saturated silicon solutions [17]. Bipolar transistors fabricated from material grown by a similar technique have also been reported [11]. MESFET's fabricated from α-SiC were first reported by Muench *et al.* [11], [18] in 1977. In this work, a thin layer of n-type SiC doped with nitrogen to a concentration of about 10^{16} cm^{-3} was deposited by liquid-phase epitaxy (LPE) on a p-type SiC crystal. The ohmic contacts were formed from an Al-Si alloy and the gate was formed by depositing thin layers of titanium and gold. Current saturation was observed and the maximum transconductance was reported to be 1.75 mS/mm for a device with a gate length of 10 μm. The first β-SiC MESFET was fabricated by Yoshida *et al.* [19]. The Al-doped p-type β-SiC layer was epitaxially grown on a p-type Si substrate, followed by growth of an unintentionally doped n-type layer. The device had high channel resistance and a maximum transconductance of only 90 μS/mm was obtained. Improved devices with transconductances of 1.7 mS/mm and 0.15 mS/mm at room temperature and 400°C were later reported by the same researchers [20]. MESFET's fabricated from β-SiC have also been reported by Kong *et al.* [21] and Kelner *et al.* [22], [23]. The transconductances for these devices were 1.6 mS/mm and 2.3 mS/mm, respectively. Junction-gate field-effect transistors [24], [25] and depletion mode MOSFET's have also been fabricated from β-SiC grown by chemical vapor deposition (CVD) on an α-SiC substrate [13], [14]. Recently, an α-SiC MESFET with a 1-μm gate length demonstrated a maximum room temperature transconductance of 25 mS/mm and a current gain cutoff frequency (f_T) of about 3 GHz [26]. Although this device has a significantly improved transconductance relative to previously reported devices, it 's performance is still limited by high parasitic resistances. Much improved performance can be expected as improved device fabrication techniques yield lower parasitics.

B. Diamond

Crystalline carbon usually exists in two structures: diamond (cubic) and graphite (hexagonal). At one atmosphere pressure and room temperature, graphite is stable while diamond is metastable. According to impurity content, diamond is grouped into four distinct types: type Ia, Ib, IIa, and IIb. Approximately 98% of natural diamonds have nitrogen aggregates and are referred to as type Ia. Diamonds in this category are usually near colorless and yellow, but they may also be brown or gray. In approximately 0.1% of natural diamonds and in most of the synthetic diamonds produced under high pressure, nitrogen is present on isolated substitutional lattice sites. This type of diamond is referred to as type Ib and the diamonds are intrinsically yellow. Diamond containing nitrogen as the major impurity with a low concentration (less than $\sim10^{18}$ cm^{-3}) is referred to as type IIa and is usually near-colorless. Type IIb diamonds contain boron as the major impurity and are usually blue or gray in color. The diamonds exhibit slightly p-type conductivity at room temperature. Semiconducting diamond is generally type IIb and is extremely rare in nature.

The electronic properties of diamond were investigated in the 1930's [1]. It was found that there were two basic types of diamond according to different optical absorption spectrum. One type was opaque in the infrared and ultraviolet spectrum while the other type was transparent. Little difference in other physical properties was observed between the two types. Natural semiconducting diamond was discovered in 1952 [27]. Custers found that type IIb diamond phosphoresced when excited by far ultraviolet radiation and showed high electrical conductivity, whereas type IIa diamond did not phosphoresce and showed low conductivity. In 1962, General Electric reported synthetic p-type semiconducting diamond from a mixture of graphite and catalyst metals (Ni, Fe, etc.) and small amounts of B, Be, or Al at high pressures and high temperatures [28], [29]. It has been shown that a concentration of atomic H exceeding that of the equilibrium concentration associated with the thermal dissociation of the reactant hydrocarbon gases is necessary to achieve diamond growth [30], [31]. The technique used in [30], [31] consisted of a chemical vapor transport process in a closed tube coupled with the passage of H_2 through an electric discharge to produce atomic H. Following this work, various approaches have been reported including AC-plasma discharge [32], heated W filament chemical vapor deposition (CVD) [33]–[35], microwave plasma assisted CVD [36]–[40], RF-plasma assisted CVD [40], [41], electron-assisted CVD [42], [43], UV-assisted CVD [44], and the use of H-ion beams [44]. Using high-pressure synthesis, Sumitomo Electric [47], [48] and DeBeers [46], [48] reported large type Ib diamond crystals of size 12 mmx12 mm.

Monocrystalline diamond films necessary for microelectronic device applications have only been grown on diamond substrates. Attempts to deposit diamond thin films on less costly substrates have produced polycrystalline layers. The best of these films have grain sizes in the range of 1–10 mm, which is approaching a useful size necessary to produce certain types of devices.

The production of device quality diamond requires techniques for introducing controlled amounts of dopant impurities. Because of the low diffusivity of most impurities in diamond, the diffusion doping technique does not work well. Diamond can be doped by ion implantation [49]–[58] or by CVD [59], [60]. Most attempts to dope diamond n-type use Li or N, although C, P, As, O, and Sb have also

Table 1 Material Parameters for Selected Semiconductors

Semiconductor	Eg(eV)	ε_r	κ(W/°K-cm) @300°K	E_c(V/cm)	$\tau_{minority}$(sec)
Si	1.12	11.9	1.5	3×10^5	2.5×10^{-3}
GaAs	1.42	12.5	0.54	4×10^5	$\sim 10^{-8}$
InP	1.34	12.4	0.67	4.5×10^5	$\sim 10^{-8}$
Diamond	5.5	5.5	30	$(1.1 - 21.5) \times 10^6$	$\sim 10^{-9}$
α-SiC	2.86	10.0	4	$(1 - 5) \times 10^6$	$\sim (1 - 10) \times 10^{-9}$
β-SiC	2.2	9.7	4	$(1 - 5) \times 10^6$	$\sim (1 - 10) \times 10^{-9}$

been reported. The electrical characteristics of synthetic n-type diamond are not currently adequate for use of this material in microwave and millimeter-wave electronic devices. Most current device effort is directed toward investigation of devices fabricated using p-type diamond. Natural semiconducting diamond is always p-type and synthetic p-type crystals can be obtained using boron doping. Boron doping by CVD [59], high pressure synthesis [29], and ion-implantation [51] yield activation energies of 0.013 eV, 0.2–0.35, and 0.27–0.3 eV, respectively.

Many applications for diamond electronic devices have been proposed [61], [62]. Preliminary development of devices using both natural [63], [64] and synthetic crystals [65]–[68] have been reported. Thermistors made of natural [63] or synthetic [66] semiconducting diamonds can operate at temperatures from 2 K to 1000 K. P-N junctions have been obtained by implanting lithium [56], [57] or arsenic [69] ions into p-type diamond crystals followed by high temperature annealing. An LED which emits in the wavelength range of 300–500 nm has been fabricated from an ion-implanted diamond [70]. The first diamond bipolar transistor was reported in 1982 [64]. The transistor exhibited very low current gain with an $\alpha \sim 0.1$. An improved n-p-n bipolar transistor with a current gain of 0.8 was reported [69] by implanting As in natural semiconducting diamond. A point-contact transistor reported by Geis [67] exhibited a small signal current gain of 2–25 and a power gain of 6–35 at room temperature. At 510°C the current gain was 0.5–1.6 and the power gain was 1.3–4.5. Initial development effort in the fabrication of diamond field-effect transistors has also been reported [71], [72]. Initial work has been on p-channel devices using boron doped diamond. A critical evaluation of the potential of diamond electronic devices has been presented by Collins [73].

III. Material And Contact Properties

The RF performance of electronic devices is determined by both the structural design of the particular device and the electronic transport characteristics of the material from which the device is fabricated. In addition, the manufacture of devices requires that low resistance ohmic contacts be fabricated between the semiconductor and external metal conductors. Rectifying contacts are also required for many devices in order to establish potential barriers for the control of currents within certain device structures. In general, contact technology is difficult on wide bandgap semiconductors, especially for ohmic contacts.

Electronic material parameters of interest are electron and hole transport characteristics as described by the charge carrier velocity-field and diffusion-field characteristics. The v-E characteristic is generally described in terms of charge carrier mobility defined from the slope of the v-E characteristic at low, ohmic electric field and the saturated velocity defined when the carrier velocity obtains a constant, field-independent magnitude. The value of electric field at which saturation occurs is also of importance since it is an indicator of how fast the charge carriers can be accelerated to the saturation value. In general, the maximum frequency of a device will be obtained with the charge carriers at their saturated velocity. The critical electric field for dielectric breakdown and the thermal conductivity of the material determine the maximum power handling capability of the device. The breakdown field places a fundamental limit on the RF power that can be converted from the dc bias and the thermal conductivity determines the ease with which unconverted dc power can be extracted from the device. The unconverted dc power produces a temperature rise in the device which, in turn, degrades the electronic charge carrier transport characteristics. The dielectric constant and bandgap are also important material properties. The dielectric constant is a factor in determining the device impedance and the bandgap defines the upper temperature limit at which the device can be safely operated. The bandgap is also instrumental in determining the resistance of the device to radiation. Wide bandgap materials are radiation resistant and diamond, in particular, is the most radiation resistant semiconductor known. In general, low dielectric constant and high bandgap are desirable material characteristics. Minority carrier lifetimes are important when designing bipolar devices such as transistors and diodes where switching speed from a conductive to nonconductive state is of importance. A comparison of some of the most important material parameters for device applications for diamond and SiC and the most commonly used semiconductors is presented in Table 1.

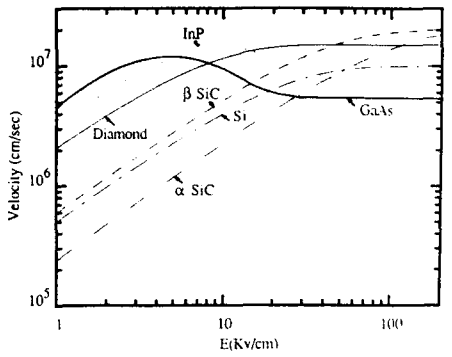

Fig. 1. Electron velocity versus electric field for several semiconductors at $N_d = 10^17cm^-3$.

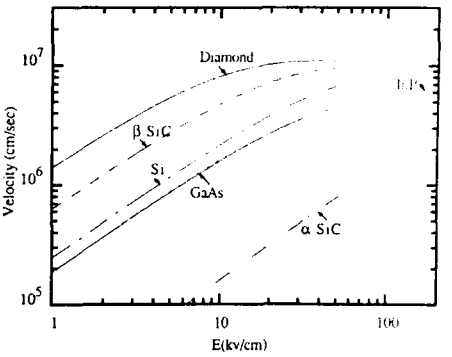

Fig. 2. Hole velocity versus electric field for several semiconductors at $N_d = 10^17cm^-3$.

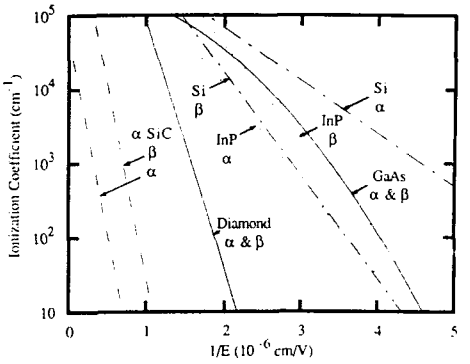

Fig. 3. Charge carrier ionization rates for several semiconductors.

Both experimental and theoretical velocity-field characteristics have been reported for diamond [74]–[77] and for SiC [74], [78], [79]. The velocity-field characteristics for both electrons and holes for several semiconductors are compared in Figs. 1 and 2. As indicated in Fig. 1, electron saturated velocity in both SiC and diamond is in the range of $(1–2)\times10^7$ cm/s. The carrier velocities for diamond and SiC in Figs. 1 and 2 are approximate since there is some uncertainty in the exact value for both the mobility and saturated velocity due to few experiments being performed. All indications are that the saturated velocity is above 10^7 cm/s in both materials. The theoretical Monte Carlo results presented in [76] for diamond indicate room temperature electron and hole saturated velocities of 1.5×10^7 cm/s and 1.2×10^7 cm/s, respectively. The electron low field mobility for an impurity concentration of 10^{17} cm^{-3} is about 1000 cm^2/V-s and 250 cm^2/V-s for diamond and α-SiC, respectively. The measured electron and hole mobilities in β-SiC have been reported to be as high as 600 and 650 cm^2/V-s, respectively, for doping concentrations of 2×10^{16} cm^{-3} [80]. The theoretical results presented in [76] indicate electron and hole mobilities of 2200 cm^2/V-s and 1900 cm^2/V-s for undoped diamond. At an impurity concentration of 2×10^{17} cm^{-3} the electron mobility is reduced to about 700 cm^2/V-s and at an impurity concentration of 10^{16} cm^{-3} the hole mobility is reduced to about 1300 cm^2/V-s. Hole mobilities in the range of 200–700 cm^2/V-s [51] and 850 cm^2/V-s [81] have been measured in boron doped diamond. The saturated velocity for holes in SiC is about 1×10^7 cm/s. The low field mobility for holes in α-SiC, however, is very low (e.g., approximately 50 cm^2/V-s) and it is very difficult to observe saturation effects. This will severely limit the use of p-type α-SiC in device applications.

The critical electric field for avalanche in diamond and SiC is significantly higher than for the commonly used semiconductors as shown in Fig. 3. The critical field significantly exceeds 10^6 V/cm in both diamond [82], [83] and SiC [84]–[87] compared to about 5×10^5 V/cm for the other semiconductors. The ionization rates for diamond indicated in Fig. 3 were determined by applying the theory of Baraff [88] to the experimental data reported in [82]. Baraff's theory describes the dependence of the ionization coefficients on the electric field by using three parameters: the Raman optical phonon energy, the ionization energy, and the carrier mean free path for optical phonon generation. Application of this theory yields ionization rates for electrons and holes in diamond that can be represented with the empirical expression

$$\alpha = \beta = 1.935 \times 10^8 \exp(-7.749 \times 10^6/E) \quad (1)$$

where α and β are the ionization rates for electrons and holes, respectively, and are assumed equal. The ionization rates for SiC indicated in Fig. 3 were calculated using the data presented by Dmitriev *et al.* [86]. Dmitriev *et al.* find 6H-SiC to be strongly anisotropic with respect to avalanche breakdown. They find the process of impact ionization to be influenced by superstructure splitting in the conduction band and that holes dominate the carrier generation. The avalanche generation by electrons is considered insignificant. Anikin *et al.* [87] also find the avalanche breakdown to be anisotropic and dominated by hole generation, but believe that the avalanche mechanism involves deep level states corresponding to residual impurities and not the conduction band superstructure. Epitaxial 6H-SiC is typically grown in the c direction and when the electric field is parallel to the c axis the ionization rates are

$$\beta = 4.65 \times 10^6 \exp(-1.2 \times 10^7/E) \quad (2)$$

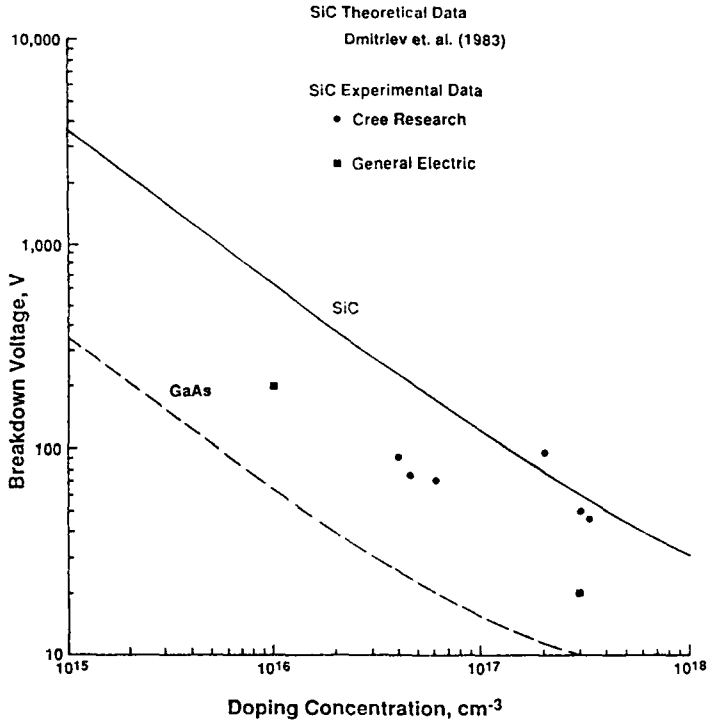

Fig. 4. Breakdown voltage versus doping for SiC and GaAs.

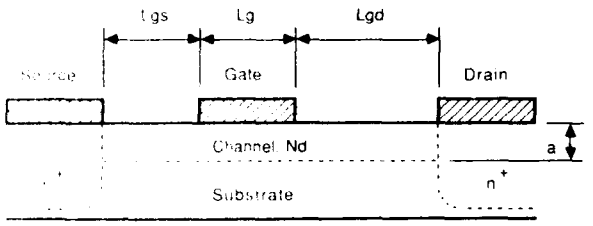

Fig. 5. Cross sectional sketch of a microwave MESFET.

and

$$\alpha = \frac{\beta}{100}. \tag{3}$$

A comparison of the breakdown voltage versus doping calculated using Dmitriev's results with experimental data is presented in Fig. 4, along with the breakdown voltage for GaAs. The data provided by Cree Research [89] is in agreement with the Dmitriev results. The General Electric data were taken from [84].

The high critical field indicates that devices fabricated from these materials will sustain large applied voltages before breakdown occurs. This factor is important when working with materials with relatively low mobilities since large electric fields are required to achieve carrier velocity saturation. Also, high breakdown voltage allows large bias to be applied with corresponding increase in RF output power. High power operation produces significant heat dissipation and thermal conductivities are important. Diamond and SiC both have high thermal conductivity as indicated in Table 1.

Both ohmic and rectifying contacts are required in device fabrication. Contact technology, however, is difficult on wide bandgap semiconductors. When metals are placed upon these materials rectifying behavior is generally obtained. Schottky contacts on diamond have been formed by vacuum evaporation of various metals [65], [67], [90], [91]. The height of the potential barrier is essentially independent of the metal due to surface pinning and has a value in the range of 1.3–1.7 eV. The room temperature reverse bias breakdown voltages for nickel-diamond [91] and tungsten-diamond [67] contacts have been measured to be 250 V and 120–350 V, respectively. A study of Schottky contacts produced from tungsten on boron-doped diamond has been reported [67]. As a result of the low ionization of the B acceptors (energy level at about 0.3 eV above the valence band) at room temperature, the turn-on voltages of the 100 μm^2 diodes exceeded 4 V and the series resistance ranged from 1 to 2 kΩ. An ideality factor of 2 and a barrier height of 1–3 V were determined from I–V measurements taken at 580°C where most of the acceptors are ionized. Similar characteristics were measured at 700°C. It has been shown that proper chemical cleaning of the boron-doped diamond surface allows the fabrication of Au-gate Schottky diodes with excellent rectifying characteristics [92]. The best rectifying p-n junctions in diamond have been produced by implantation of Li ions into p-type crystals followed by annealing at 1430°C [57], [93]. Good rectifying contacts to SiC have been formed by deposition of Ti/Au [11] and thermal evaporation of Au [10]. Gold,

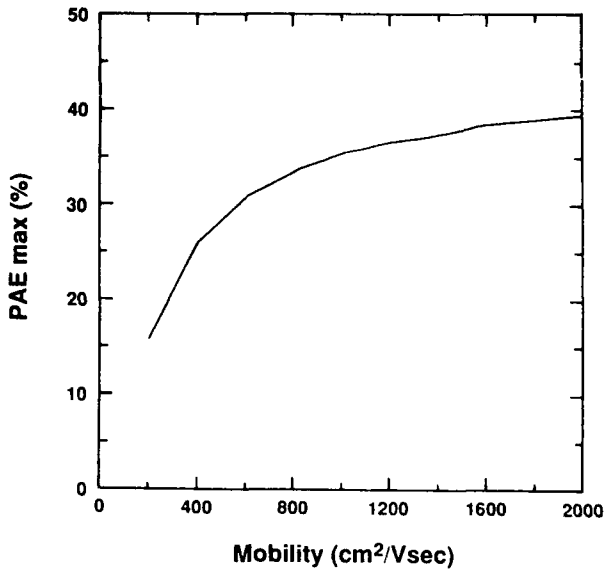

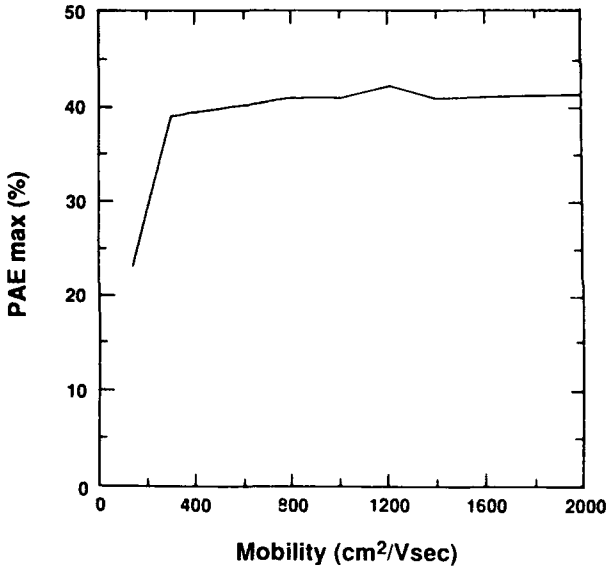

Fig. 6. RF performance versus charge carrier low-field mobility for MESFET's biased at V_{ds} = 20V for a class A operation at 10 GHz with (a) 1 μm gate length, and (b) 0.5 μm gate length.

which is the most successful Schottky material for SiC has several disadvantages including poor adherence to SiC and reaction with SiC above 400°C. There is interest in refractory metals and refractory metal silicides (e.g., $PtSi_x$) for use as Schottky barriers on SiC. Rectifying p-n junctions in SiC are formed by in situ doping during growth or by ion-implantation. Typical p-type and n-type dopants are B or Al and P or N, respectively. Diodes typically exhibit high reverse voltages with low leakage current, high current carrying capability and fast switching speed. High temperature operation is possible and no significant degradation in junction characteristics are observed, at least to 350°C. Due to the large bandgap of SiC the build-in potential is relatively high and has a value in the range of 2.4–2.5 V, compared to 0.7–1.0 V obtained with GaAs and Si. Ideality factors for SiC junctions are generally about 1.6–2.0, indicating a significant generation-recombination current mechanism. The absence of a pure diffusion current (which would be indicated by an ideality factor approaching unity) is consistent with the low intrinsic density of $n_i \sim 10^{-5}$ cm^{-3} characteristic of SiC. Due to the high critical field SiC diodes have high breakdown voltage (e.g., V_B>400 V are easily achieved). Reverse leakage currents can be very low due to the wide bandgap and reverse saturation current densities in the range $J_s \sim 10^{-14}$ A/cm^2 have been obtained.

Ohmic contacts to diamond have demonstrated very high electrical resistance due to the large potential barrier of approximately 4 eV at the diamond/metal interface [94]. Diamond is one of the least reactive of the elements and contact formation is hindered by poor adherence which contributes to high contact resistance. Most initial work with diamond devices used techniques such as tungsten point contact or silver paint to contact the semiconductor. The resulting contacts were characterized with high resistance (e.g., ~kΩ and larger). More recent work has obtained much improved ohmic contact performance using annealed Ta/Au and Ti/Au deposits on polished diamond surfaces [95], [96]. A thin film of a strong carbide forming metal is deposited on the semiconducting diamond surface and annealed to cause a chemical reaction between the diamond and metal. Metals such as tantalum, molybdenum, and titanium can be deposited and annealed to form reduced resistance contacts that adhere well to the diamond. It has also been reported that exposure of the diamond film surface to a hydrogen plasma results in the formation of a conductive layer which can be used to obtain linear I-V characteristics [92]. The contact resistivity obtained on diamond, however, remains large and must be reduced if high performance electronic devices are to be fabricated. Ohmic contacts to SiC can be formed by deposition of metals such as Ni, Ag, Ta, W, Mo, and Ti. Sputtered $TaSi_2$ has provided a good ohmic contact to n-type β-SiC; however, e-beam evaporation of elemental Ta has produced ohmic contacts on this material with contact resistivities of $Rc \sim 10^{-5}$ Ω-cm^2, which is an order of magnitude better than obtained using the $TaSi_2$. Contacts to α-SiC are not well established, although sintered Ni and a 94% Au/6% Ta alloy have been used. This material produces contact resistivities in the range of $Rc \sim 10^{-3}$ Ω-cm^2.

IV. Diamond And SiC Electronic Devices For High Frequency Power Applications

In order to investigate the RF performance potential of diamond and SiC electronic devices, computer simulations were performed. The investigation utilizes physically based, theoretical computer models for the MESFET [97] and IMPATT diode [98]. The models have demonstrated excellent accuracy in predicting the RF performance of a variety of experimental devices fabricated from Si, GaAs, and InP. The models require material parameters, device designs, and operating conditions as input data and provide

calculations of the dc and RF performance. The bipolar simulations were performed using a commercially available nonlinear device/circuit simulator [99]. The simulator requires that an equivalent circuit be established and, for this work, the equivalent circuit element values were determined from design calculations determined from the physical operation of the device. Device structures were designed to produce optimum RF output power and power-added efficiency at a variety of microwave and millimeter-wave frequencies. The results of the calculations indicate the RF potential of the wide bandgap materials for use in these applications. Only power applications were considered and no attempt was made to consider the noise performance of the devices. However, due to relatively low carrier mobility of the wide bandgap materials compared to GaAs, the noise performance of diamond and SiC devices is expected to be inferior to GaAs devices.

A. MESFET's

The MESFET simulator [97] used in this work was originally developed for studies of GaAs devices. The device model is based upon efficient solutions of the basic semiconductor device equations and, therefore, contains a comprehensive description of the physical operation of the device. Major physical phenomena known to be of importance to device operation are included. The model accepts as input information material data such as charge carrier transport characteristics, breakdown parameters, thermal conductivity and dielectric constant, as well as device design information such as geometry, doping profile data and contact characteristics. Bias, RF circuit, and operating conditions must also be supplied.

For this work, the simulator was supplied with material parameters for SiC and diamond and MESFET structures were designed that resulted in optimized RF performance. The high frequency performance was determined for devices embedded in a realistic RF circuit. Therefore, impedance matching considerations were significant in determining device size limitations for maximum RF output power. Similar devices fabricated from GaAs were also investigated for comparison purposes.

A cross section of the MESFET device structure investigated is shown in Fig. 5. The MESFET has two ohmic contacts (the source and drain) separated by some distance, usually in the range of 3 to 10 μm. A rectifying Schottky contact (the gate) is located between the two ohmic contacts. Typically, the gate length is on the order of 0.1 to 2 μm for modern microwave devices. The width of the device scales with frequency and typically ranges from about 50 μm for millimeter wave devices, to 1–10 mm for power microwave devices. All three contacts are located on the surface of a thin conducting layer (the channel) which is located on top of a high resistivity, nonconductive substrate to form the device. In operation, the drain contact is biased at a specified potential (positive drain potential for an n-channel device) and the source is grounded. The flow of current through the conducting channel is controlled by negative dc and superimposed RF potentials applied to the gate, which modulate the channel current and provides RF gain.

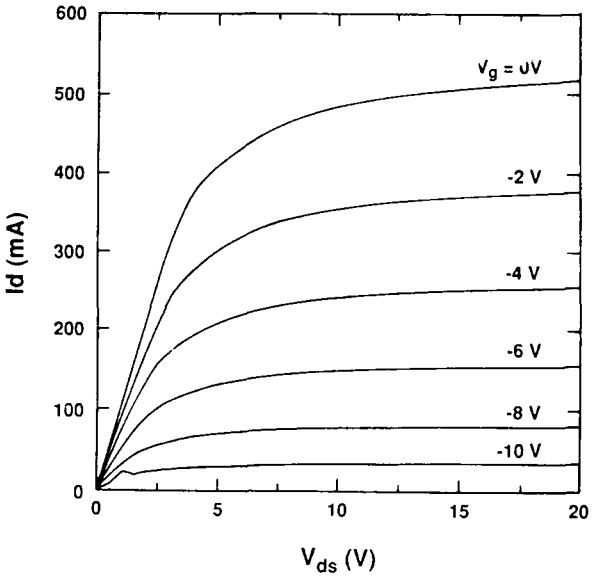

Fig. 7(a). I-V characteristics for a diamond MESFET (L_g = 0.5 μm, W = 1 μm).

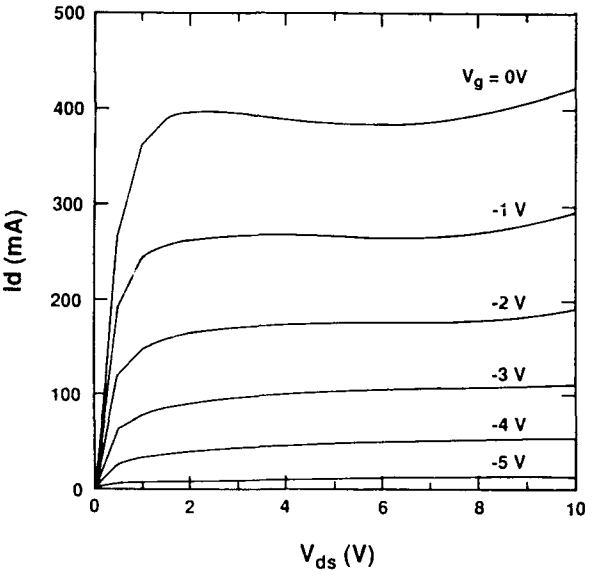

Fig. 7(b). I-V characteristics for a GaAs MESFET (L_g = 0.5 μm, W = 1 μm).

The parameters used for the diamond and SiC MESFET's and also for a similar GaAs device are indicated in Table 2. The diamond MESFET is assumed to have a Schottky gate contact fabricated using gold. The drain and source contacts are assumed ohmic with a specific contact resistivity of Rc~10–4 Ω-cm^2. A contact resistivity of this value is sufficient for microwave power applications where large contact size helps reduce total contact resistance. However,

Table 2 MESFET Parameter Values Used in the Simulations

Parameter	Diamond	Value	
		α-SiC	GaAs
L_g	(0.5 – 1) μm	(0.5 – 1) μm	0.5 μm
L_{ds}	3.5 μm	3.5 μm	3.5 μm
L_{gs}	1 μm	1 μm	1 μm
N_d	4×10^{17} cm^{-3}	2.4×10^{17} cm^{-3}	2.0×10^{17} cm^{-3}
a	0.15 μm	0.25 μm	0.23 μm
W	1 mm	1 mm	1 mm
Φ_{bi}(Au)	1.71 eV	1.95 eV	0.6 eV
R_C	$\sim 10^{-4}$ Ω – cm^2	$\sim 10^{-5}$ Ω – cm^2	$\sim 10^{-6}$ Ω – cm^2

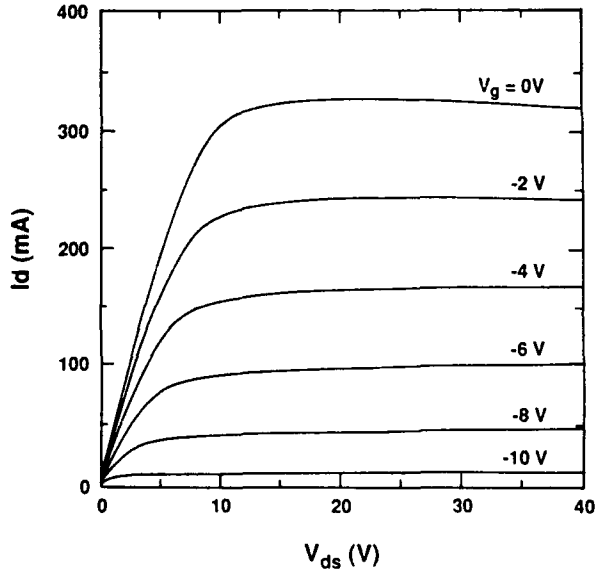

Fig. 8(a). I-V characteristics for a SiC MESFET ($L_g = 1$ μm, $W = 1$ mm).

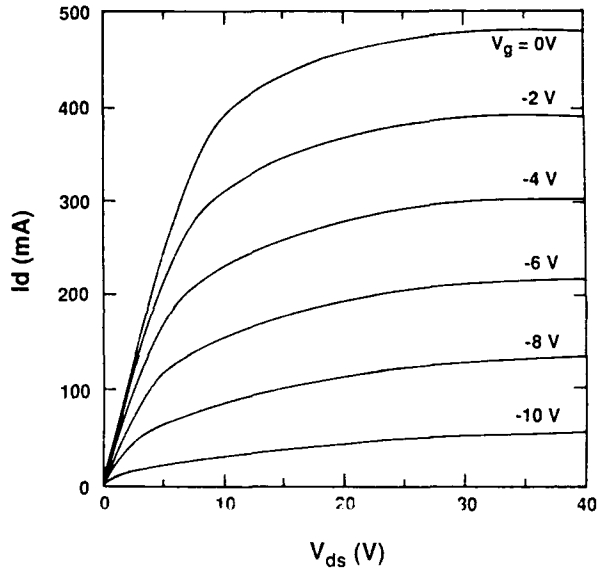

Fig. 8(b). I-V characteristics for a SiC MESFET ($L_g = 0.5$ μm, $W = 1$ mm).

for millimeter-wave devices the contact resistivity will need to be reduced to approximately Rc~10^{-6}–10^{-7} W-cm^2 in order to produce low resistance contacts. Contact size scales with frequency and reduced contact area is required for mm-wave operation.

Mobility directly affects channel current and, therefore, RF performance. The effect of varying mobility upon the maximum power-added efficiency of power MESFET's is illustrated in Fig. 6(a) and 6(b), respectively for devices with 1 μm and 0.5 μm gate lengths biased with a drain voltage of 20 V for class A operation at 10 GHz. The calculations shown in Fig. 6 apply to both SiC and diamond MESFET's. As indicated, mobility has a significant effect upon the RF performance of the device, especially when the mobility is low. The power-added efficiency increases with mobility until a critical value of about 1500 cm^2/V-s is reached for the 1-μm gate length device. Mobilities above this value do not result in significantly improved RF power performance. The limiting effect of mobility is related to the magnitude of the electric field in the channel under the gate electrode. This region consists of essentially two regions: a low electric field region where carrier transport is dominated by the mobility (ohmic region) and a high field region where saturated carrier velocity occurs. The boundary between these two regions depends upon the device structure, primarily gate length and bias conditions, as well as the magnitude of the mobility. Power devices are ypically operated at high drain bias. A high electron mobility results in a minimized ohmic region under the gate electrode since the carriers are rapidly accelerated by the high channel field. This allows the channel current to be determined by the saturated velocity

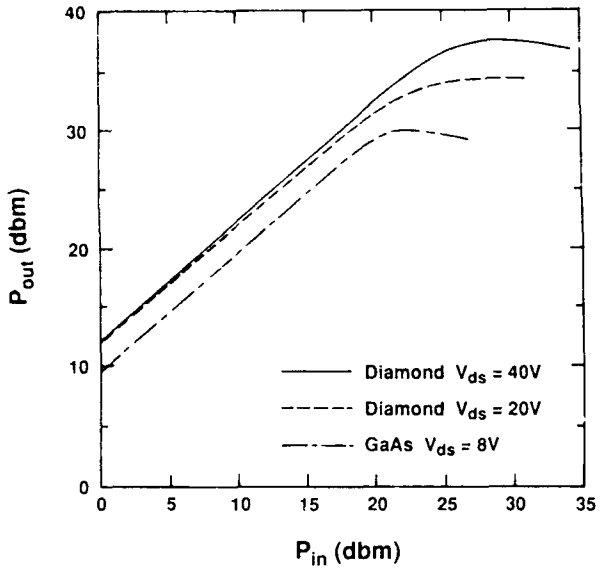

Fig. 9(a). RF output power versus input power for diamond and GaAs MESFET's (F=10 GHz, L_g=0.5 μm, W=1 mm, Class A).

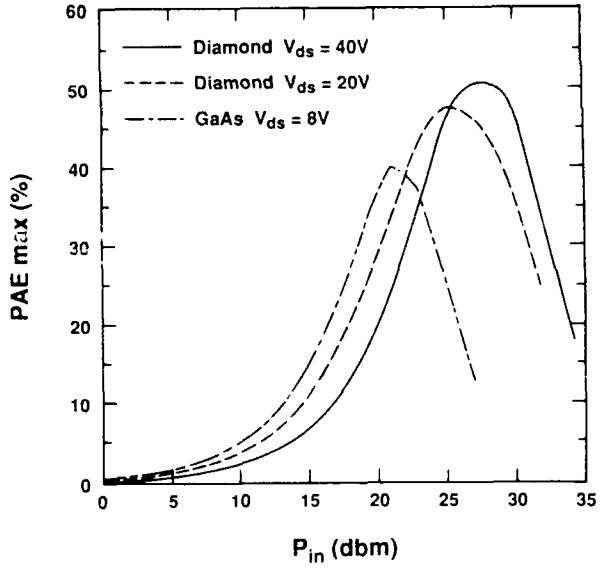

Fig. 9(b). Power-added efficiency versus input power for diamond and GaAs MESFET's (F=10 GHz, L_g=0.5 μm, W=1 mm, Class A).

and thereby maximized. For mobilities above about 1500 cm^2/V-s essentially the entire channel under the gate is at or above the saturation field. Therefore no improvement is observed for increased values of mobility.

For mobilities below about 1000 cm^2/V-s RF performance degradation in the 1-μm gate length device occurs. The degradation results from an increased ohmic region in the channel which limits the channel current. The degradation increases with reductions in mobility and, for mobility

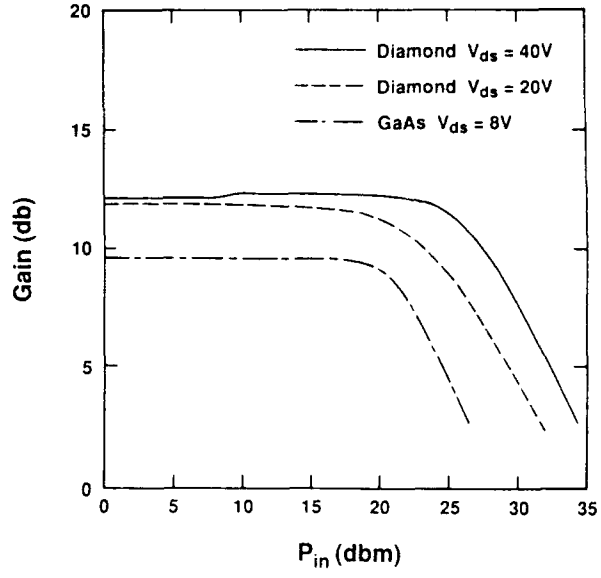

Fig. 9(c). Gain versus input power for diamond and GaAs MESFET's (F=10 GHz, L_g=0.5 μm, W=1 mm, Class A).

in the range of about 250 cm^2/V-s, significant degradation in RF performance is observed as indicated in Fig. 6(a). At this value of mobility a large portion of the conducting channel is in the ohmic region, thereby minimizing the effects of velocity saturation and reducing channel current.

The severe degradation shown for the 1-μm gate length device for a mobility of 250 cm^2/V-s could be reduced by techniques designed to increase the magnitude of the electric field in the channel. For example, a reduction in gate length is known to increase channel electric field and produce increased channel current. This is the technique generally employed in the fabrication of GaAs devices [100]. The effect of reducing gate length to 0.5 μm is shown in Fig. 6(b). The greater channel electric field reduces the critical mobility required to achieve saturation to a value of about 300 cm^2/V-s.

Increased electric field also results from increased drain bias. For class A operation the drain bias can be increased until it is about 40–50% of the gate-drain breakdown voltage. For modern Si and GaAs microwave devices the relatively low breakdown field limits breakdown voltages to about 20–25 V and drain bias voltages to the range of 8–12 V. The high breakdown fields of diamond and SiC should permit these devices to be biased at much higher voltages. This will, in fact, be necessary if efficient RF performance is to be obtained.

Low charge carrier mobility also degrades device performance through increased parasitic resistances. Both the drain (Rd) and source (Rs) resistances are increased in direct proportion to mobility. This effect is very significant for very high frequency (mm-wave) and/or low noise devices, or digital logic MESFET's, which are fabricated with relatively short gate widths. Power MESFET's, however, have large gate widths which, due to aspect ratio

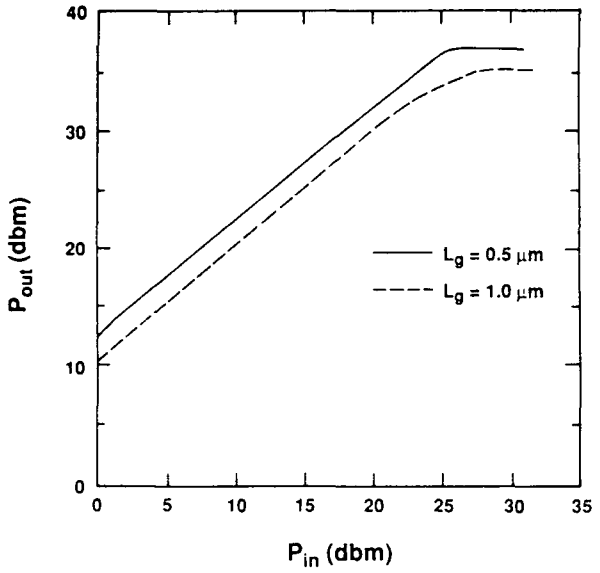

Fig. 10(a). RF output power versus input power for 0.5 μm and 1 μm gate length SiC MESFET's (F=10 GHz, W=1 mm, Class A).

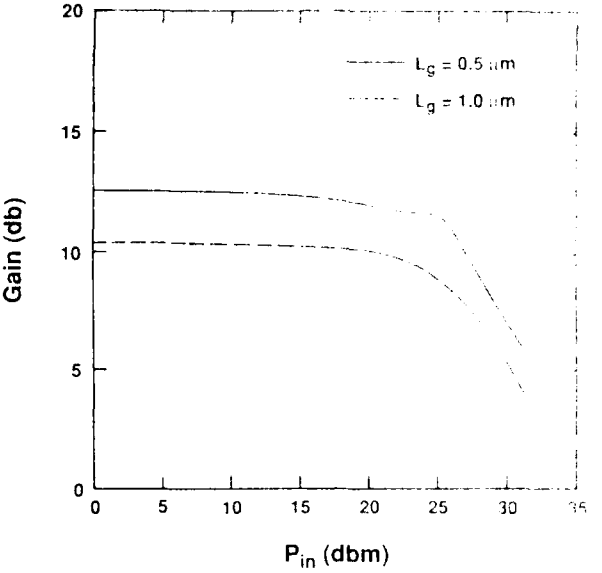

Fig. 10(c). Gain versus input power for 0.5 μm and 1 μm gate length SiC MESFET's (F=10 GHz, W=1 mm, Class A).

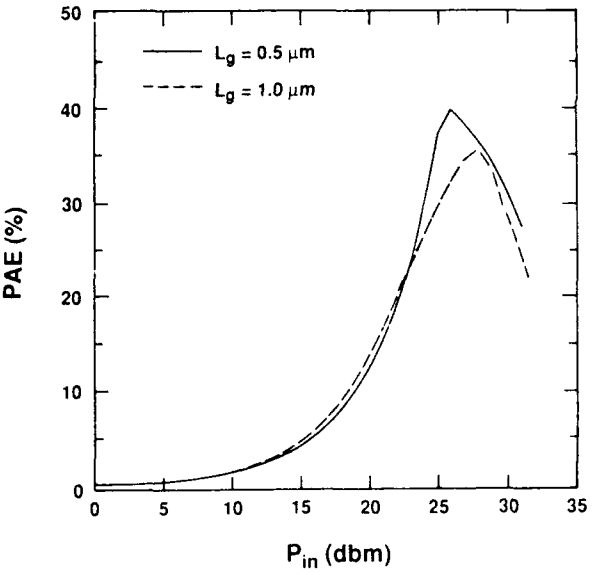

Fig. 10(b). Power-added efficiency versus input power for 0.5 μm and 1 μm gate length SiC MESFET's (F=10 GHz, W=1 mm, Class A).

considerations, minimize the significance of low charge carrier mobility. The parasitic resistances are typically sufficiently low due to the wide gate width that even order of magnitude decreases in mobility do not seriously degrade device performance.

In order to determine the RF capability of diamond and SiC MESFET's the device structures were optimized to produce a maximum power-added efficiency at an input drive level sufficient to produce a one dB compression in the gain. The devices were biased for class A operation at a drain current of $I_{ds} = I_{dss}/2$, where I_{dss} is the channel current with zero bias applied to the gate electrode. The calculations were performed for an operating frequency of 10 GHz with the device embedded in an RF circuit and the circuit was tuned to obtain the desired performance.

A comparison of the dc I-V characteristics obtained for the diamond and GaAs devices are shown in Fig. 7(a) and 7(b), respectively. The maximum transconductances are g_m = 76 mS/mm and g_m = 190 mS/mm for the diamond and GaAs devices, respectively. The lower transconductance of the diamond MESFET is due to a larger pinch-off voltage. The diamond device, however, produces a larger current than the GaAs device for similar bias voltages. This results from the greater saturation velocity of the charge carriers in diamond. In order to achieve current saturation, the diamond device requires larger drain voltages than the GaAs device. This is due to the lower mobility (by about a factor of six) of the charge carriers in diamond as compared to GaAs. The magnitude of the channel current is an indicator of the power capability of the device and the greater current of the diamond device is expected to translate into improved RF power performance. The dc I-V characteristics for the SiC device are shown in Fig. 8. One device is fabricated with a gate length of 1 μm, and the other device has a gate length of 0.5 μm. The maximum transconductances for the two devices are g_m = 37 mS/mm and g_m = 46 mS/mm. The lower mobility of the charge carriers in SiC limit the channel current to values less than can be obtained with diamond for comparable gate length. Drain bias voltages in the range of 5–10 V are required to achieve current saturation.

A comparison of the RF power capability of the diamond and GaAs devices is shown in Fig. 9. The RF power, power

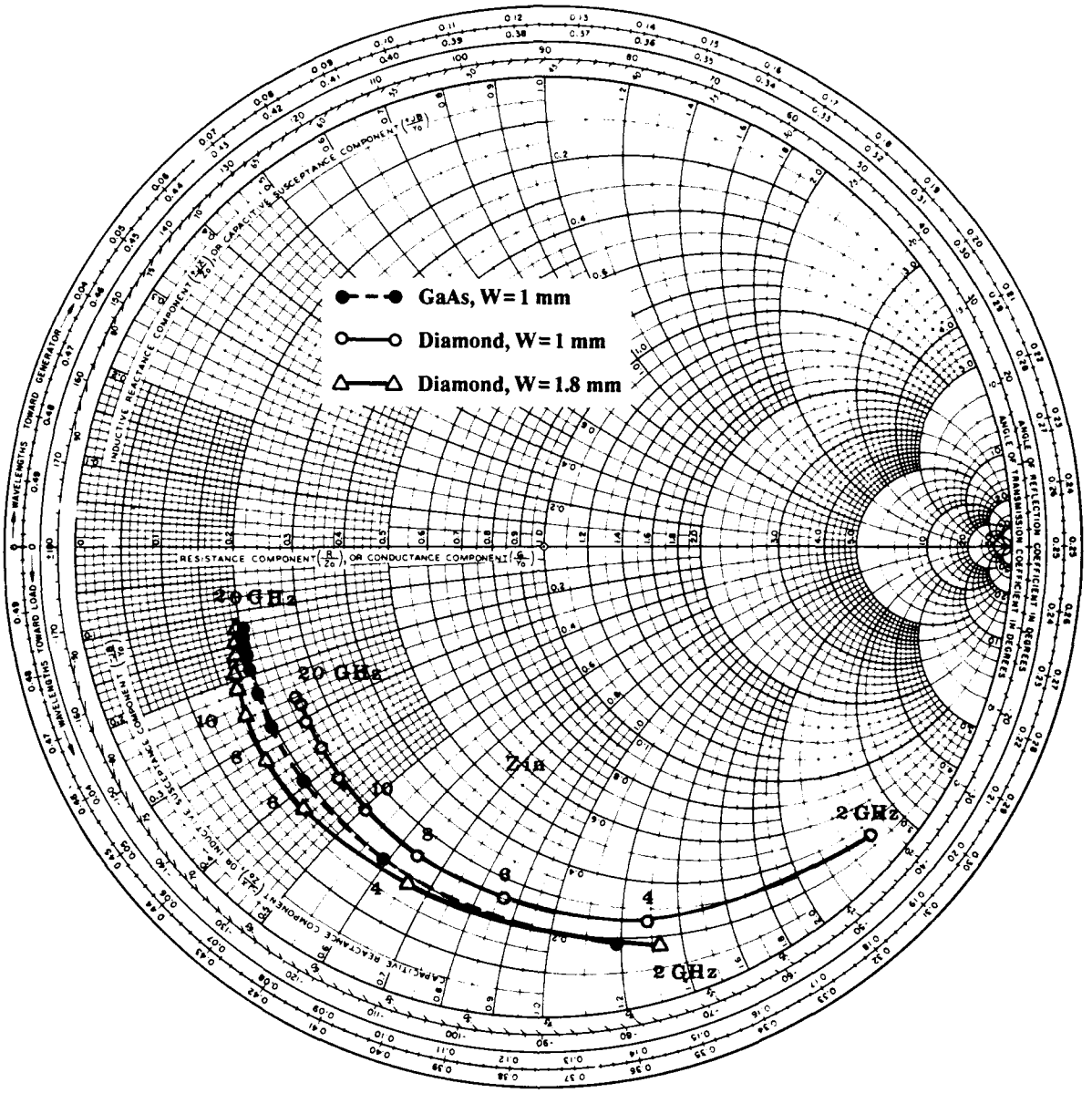

Fig. 11. Small-signal input impedances for diamond and GaAs MESFET's.

added efficiency, and gain are shown in Figs. 9(a), 9(b), and 9(c), respectively. The diamond MESFET performance is determined for drain bias voltages of $V_{ds} = 20$ and 40 V. The GaAs device is operated at a drain bias of $V_{ds} = 8$ V. The gate-drain breakdown voltage is critical in determining the magnitude of drain bias that can be applied. For GaAs devices with 1-μm gate lengths, the gate-drain breakdown voltage is typically in the range of 15–20 V. Generally, a MESFET can only support a drain bias of about 40–50% of the breakdown voltage. Since the breakdown field in diamond is at least twice and as much as five times that in GaAs, gate-drain breakdown voltages in the range of 40–100 V should be possible. For this reason, the diamond device was biased at the higher drain potentials. The higher drain voltages result in improved RF performance as indicated in Fig. 9(a). The diamond device produces about 6 W/mm of gate periphery RF power compared to about 1 W/mm of RF power for the GaAs device. The power-added efficiencies for the two devices are comparable and in the range of 40–50%. The diamond MESFET is more efficient (about ten percentage points) than the GaAs device. The linear gain of the diamond device is about 2–3 dB greater than that for the GaAs device. Also, the dynamic range (i.e., the range of input power for which the gain is constant) for the diamond device is about 5 dB greater than that for the GaAs device. The greater linear operating range of the diamond device produces lower magnitudes of the harmonic frequencies when the device is driven into saturation. This indicates that diamond devices may be useful in applications that

Table 3 GaAs and Diamond MESFET Operation at 10 GHz Device Input Impedance Matched to 1 Ω

	GaAs	Diamond
Input Impedance (Ω)		
Z_{in} for W = 1 mm	10-j11.5	12.5-j25
Z_{in} for max. width	1-j1.15 (10 mm)	0.7-j1.39 (18 mm)
RF Power at Max. Width (W)	8	225
Thermal Resistance (°C/W)	10.2	1.8
P_{diss} (W)	15.8	187
Power-Added Efficiency (%)	30	36
Channel Temp. Increase (°C)	113	215

require linear performance, such as receiver input stages.

Similar calculations performed for SiC MESFET's with 1-μm and 0.5-μm gate lengths are shown in Fig. 10. The RF output power, power-added efficiency, and gain for class A operation at 10 GHz are shown in Figs. 10(a), 10(b), and 10(c), respectively. The devices were biased with $V_{ds} = 40$ V. The SiC device produces about 5 W/mm of RF power which also indicates improved RF performance of the SiC MESFET compared to the GaAs device. The lower RF power of the SiC MESFET compared to the diamond device is due to the reduced value of low field mobility and the corresponding reduction in the conducting channel current. The SiC MESFET is also capable of good power-added efficiency (greater than 30%) and good gain. In particular, significant improvement in the RF performance of the device is observed for reduced gate length designs. High performance MESFET's fabricated from SiC will require submicron lithography. The gate-drain breakdown voltage of the SiC device should be comparable to or greater than that for the diamond device. The thermal conductivity of SiC, however, is only about an eighth of that for diamond and this will limit the power performance of SiC devices to power levels less than can be achieved with diamond.

The calculations presented assumed a gate width of 1 mm. While typical of device designs intended for *X*-band (i.e., 8–12 GHz) microwave applications, this does not represent the maximum device width that can be effectively utilized. The maximum gate width possible scales inversely with frequency and is determined by impedance matching, as well as dc power dissipation considerations. Increasing the gate width increases the RF current and, therefore, the RF power that is generated. However, as the device width is increased the input impedance of the device is reduced. About the lowest impedance that can be matched to a 50-Ω circuit is 1 Ω. This criterion can be used to obtain an estimate of the maximum RF power capability of the device by increasing gate width until the input impedance is reduced to 1 Ω. The resulting device design can then be analyzed to determine the RF capability limits of the device. The results of this type of analysis are presented in Table 3 for both diamond and GaAs MESFET's. The phase velocity in diamond is significantly lower than that in GaAs due to the lower dielectric constant. An increased device impedance results. For example, the input impedances for diamond and GaAs MESFET's with 1-mm gate width are indicated on the Smith Chart shown in Fig. 11. The impedance loci are for a frequency band from 2–20 GHz. To reduce the diamond MESFET input impedance to a level equivalent to that for the GaAs MESFET allows the diamond gate width to be increased to 1.8 mm. The increased gate width translates directly into increased channel current and RF power. As indicated in Table 3, for operation at 10 GHz, the maximum gate width in GaAs is 8 mm and 18 mm in diamond. Both devices produce power-added efficiencies greater than 30%. Too large a gate width will, of course, produce channel heating, which will limit the RF performance of the device. The thermal resistances for the devices were calculated and used to determine the channel heating. At the power levels indicated in Table 3, the temperature rise in the GaAs device is 113°C and 215°C in the diamond device. Both materials are able to support these temperatures. The maximum allowed channel temperature before damage occurs is approximately 200°C for GaAs and possibly in the range of 700°C–1000°C for diamond.

The operation of the SiC MESFET as a function of gate width was also investigated. In this study, however, the operation of the device embedded in an RF circuit was simulated and the gate width was increased until a degradation in PAE of between 20–25% was observed. This limit is arbitrary, but allows RF operation with good RF output power and PAE. Large gate widths can result in RF performance degradation due to distributed transmission line effects. To minimize these effects multiple gate fingers are used. A rule of thumb to avoid distributed effects is to design the maximum gate finger length to be no more than 1/20 of a wavelength. Gate finger length, therefore, depends upon the operation frequency and for the 10 GHz SiC MESFET is 250 μm.

The calculated dc I-V characteristics for the 10 GHz device are shown in Fig 12. With a gate width of 16 mm, the device has an I_{dss} of about 7.7 A and a pinch-off voltage

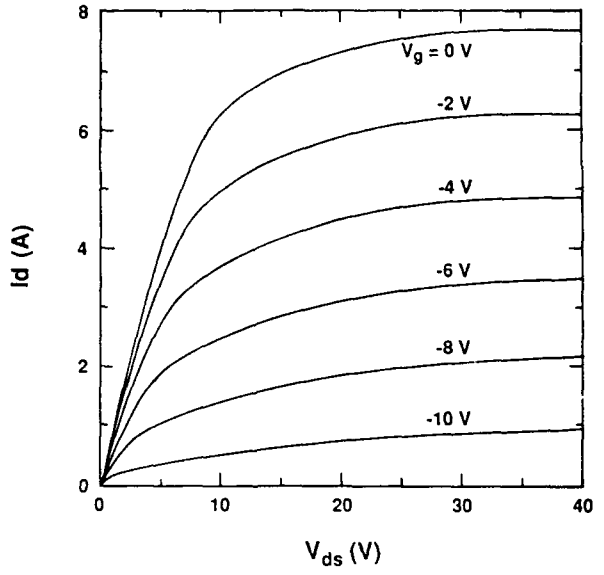

Fig. 12. I-V characteristics for a SiC MESFET with $L_g = 0.5$ μm and $W = 16$ mm.

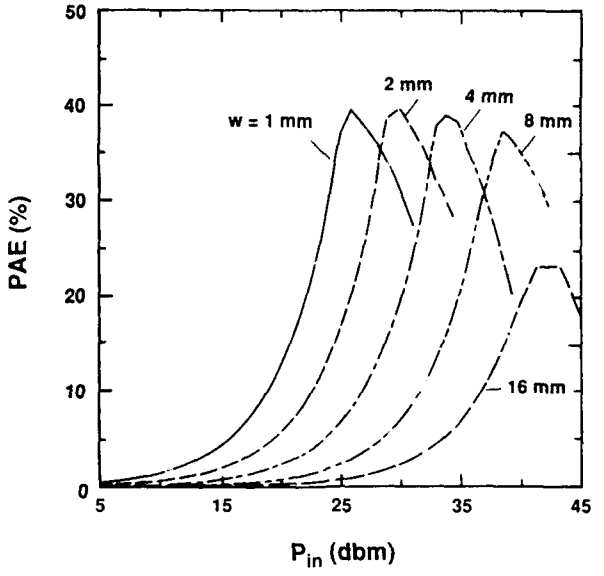

Fig. 13(b). Power-added efficiency versus input power for SiC MESFET's with $L_g = 0.5$ μm and gate widths from 1–16 mm ($F = 10$ GHz, $V_{ds} = 40$ V, Class A).

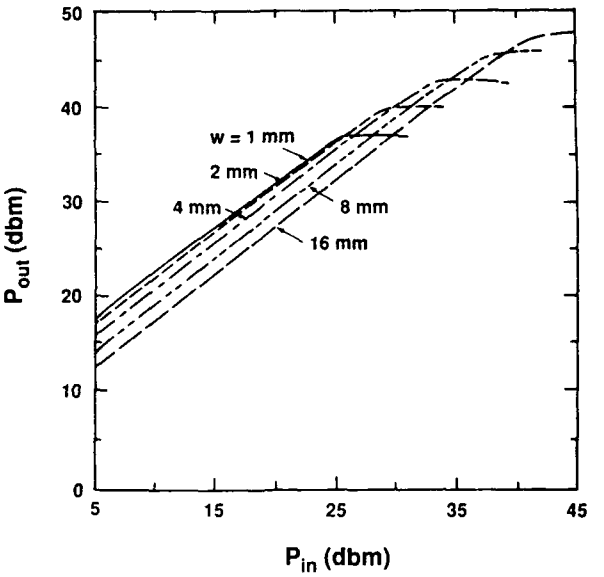

Fig. 13(a). RF output power versus input power for SiC MESFET's with $L_g = 0.5$ μm and gate widths from 1–16 mm ($F = 10$ GHz, $V_{ds} = 40$ V, Class A).

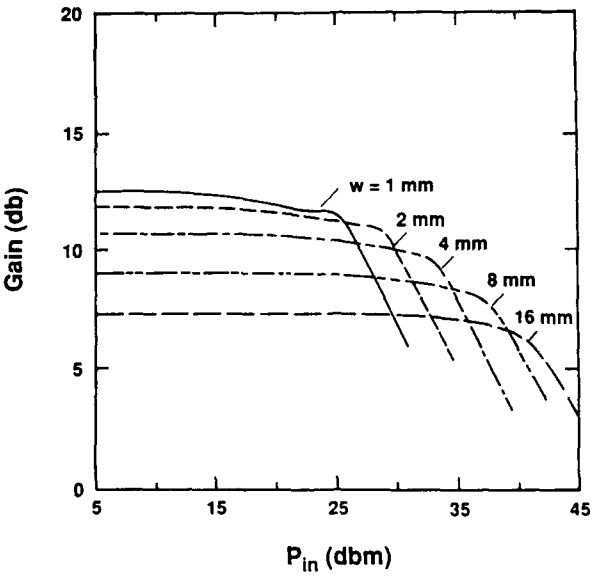

Fig. 13(c). Gain versus input power for SiC MESFET's with $L_g = 0.5$ μm and gate widths from 1–16 mm ($F = 10$ GHz, $V_{ds} = 40$ V, Class A).

of $V_p = -11.6$ V. The large gate width results in a reduced maximum transconductance of 30 mS/mm, but good RF output power is obtained. For RF operation the device was biased at a drain voltage of 40 V and a channel current of 3.4 A. The RF output power, PAE, and gain are shown in Figs. 13(a), 13(b), and 13(c), respectively. The device produces a maximum RF output power of 65 W, a PAE of 23.4%, and a linear gain of 7.3 dB. The normalized RF output power is about 4 W/mm.

If efficient operation is to be obtained the excess dc power must be extracted from the device. The ability of the device to dissipate excess energy is indicated by the thermal impedance or resistance of the device. The thermal resistance is a measure of the ease with which heat can flow from the conducting channel to the heat sink and it can be calculated from heat flow arguments or measured using a combination of pulse and dc operating conditions. Since at 300 K the thermal conductivity of SiC is about 4 W/K-cm compared to 1.5 and 0.54 W/K-cm for Si and GaAs, respectively, significantly reduced thermal resistance should result. For example, a 1-mm gate width

GaAs power MESFET typically has a thermal resistance of about 50°C–60°C/W. The largest contribution to the thermal resistance results from heat flow through the semi-insulating substrate. The resistance to heat flow from the conducting channel into the substrate is generally small, and the resistance to heat flow from the substrate into the heat sink can be minimized by using a good thermal conductor for the heat sink. Typically gold plated copper is used, but if improved thermal resistance is desired type II diamond heat sinks can be employed. Ceramics with good thermal characteristics such as metallized BeO are also used.

In order to minimize the thermal resistance of GaAs power MESFET's the semi-insulating substrate material is generally thinned to a thickness in the range of 50 μm. This results in a thermal resistance of about 60°C/W for a 1-mm gate width device. Based upon its significantly larger thermal conductivity a comparable SiC MESFET is calculated to have a thermal resistance of about 7°C–8°C/W. For a 40 V drain bias and a drain to source current of $I_{ds} = I_{dss}/2$ a channel temperature rise of approximately 60°C–80°C would result.

It should be noted that increased gate width will result in lower thermal resistance due to the larger area between the device channel and the heat sink. The thermal resistance will scale inversely with gate width. It should also be noted that SiC devices have demonstrated operation at temperatures exceeding 350°C without significant degradation. In fact, SiC devices often demonstrate increased currents at elevated temperatures. This is thought to be due to increased activation at the higher temperatures which compensates for the decreased charge transport characteristics.

The RF performance of the SiC MESFET as a function of temperature is indicated in Fig. 14. The RF performance is calculated for device thermal resistances of 0°C/W, 5°C/W, and 10°C/W. The dissipated dc energy causes a temperature rise in the conducting channel and, since charge carrier transport varies inversely with temperature, reduced mobility and carrier velocity result. The degraded charge carrier transport produces a reduced channel current and a corresponding degradation in RF performance. For a thermal resistance of 10°C/W the RF power, maximum PAE, and linear gain are reduced by about 1 dB, 5 percentage points, and 2.5 dB, respectively.

The frequency performance of the devices was also examined. Frequency performance scales directly with saturation velocity and, since diamond and SiC have a higher saturation velocity than GaAs, devices fabricated from these materials may be expected to operate at higher frequencies. The results of the calculations are shown in Fig. 15. This figure presents a comparison of the one db compressed RF power for GaAs, SiC, and diamond MESFET's as a function of frequency. The devices are redesigned and scaled for several frequencies to determine the curve. The performance of the GaAs devices are both experimental and calculated. That is, the model accurately predicts the performance obtained experimentally. The experimental results represent the state-of-the-art for GaAs MESFET's. The diamond and SiC device results were determined using

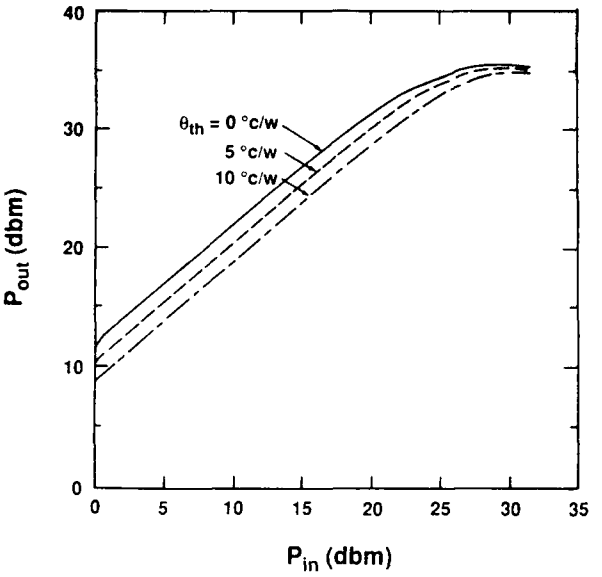

Fig. 14(a). RF output power versus input power for an SiC MESFET for various values of thermal resistance (F=10 GHz, $L_g = 1$ μm, $W = 1$ mm, $V_{ds} = 40$ V, Class A).

the simulator. The calculations predict that at 100 GHz about 1 W and 300 mW of RF power can potentially by obtained from diamond and SiC MESFET's, respectively. This performance is significantly better than possible with GaAs MESFET's.

B. IMPATT Diodes

The IMPATT diode has proven to be a useful device for the generation and amplification of RF energy from the microwave to the high mm-wave spectrum. Although in recent years the GaAs MESFET has taken over many of the systems applications in the microwave spectrum, IMPATT's are still used at mm-wave frequencies. The basic structure for a double-drift IMPATT diode is shown in Fig. 16. The device consists of a p-n junction, sandwiched between two low doped "drift" regions. In operation, the device is biased into avalanche breakdown of the p-n junction. The electron and hole densities are driven by the electric field and travel in opposite directions through the corresponding drift regions to the device contacts. The avalanche process produces approximately a 90° phase shift in the RF current relative to the RF voltage. The delay through the drift regions causes an additional inductive phase delay which, when added to that due to the avalanche process, results in a total delay exceeding 90°, thereby generating a negative resistance. When placed in a resonant circuit, the device oscillates. The double-drift structure is generally employed for high frequency applications since it operates basically as two back-to-back diodes. Device impedance levels are increased, thereby permitting larger area devices and higher output power to be obtained. A disadvantage of the double-drift structure is that the most significant dc power dissipation occurs in the avalanche

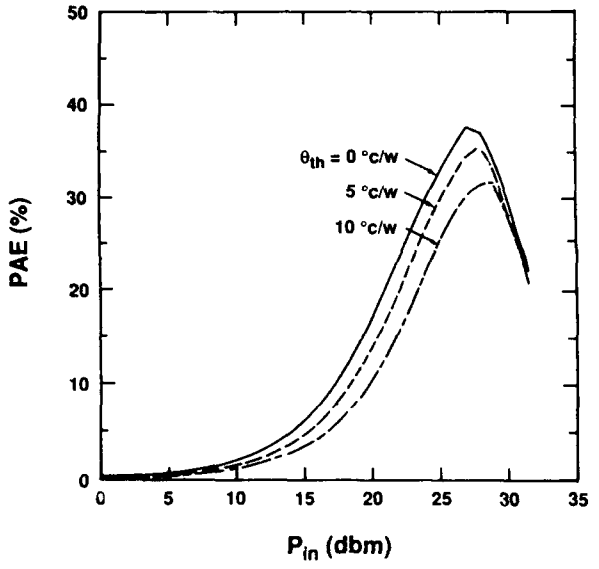

Fig. 14(b). Power-added efficiency versus input power for an SiC MESFET for various values of thermal resistance (F=10 GHz, L_g = 1 μm, W = 1 mm, V_{ds} = 40 V, Class A).

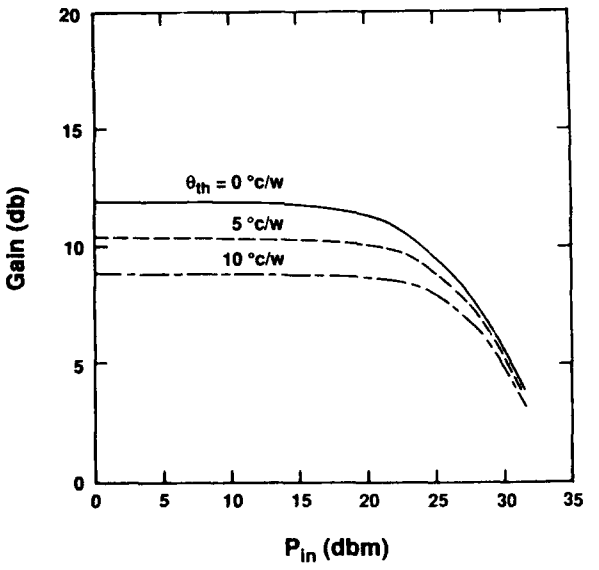

Fig. 14(c). Gain versus input power for an SiC MESFET for various values of thermal resistance (F=10 GHz, L_g = 1 μm, W = 1 mm, V_{ds} = 40 V, Class A)

region which is located inside the device. The problem is alleviated for mm-wave devices due to thin drift regions, which scale inversely with frequency.

When properly designed, the device will operate with the electric field within the device above that required to achieve charge carrier velocity saturation. The low field mobility is only important in that it determines if velocity saturation conditions can be achieved and is also fundamental in determining the parasitic resistances due to

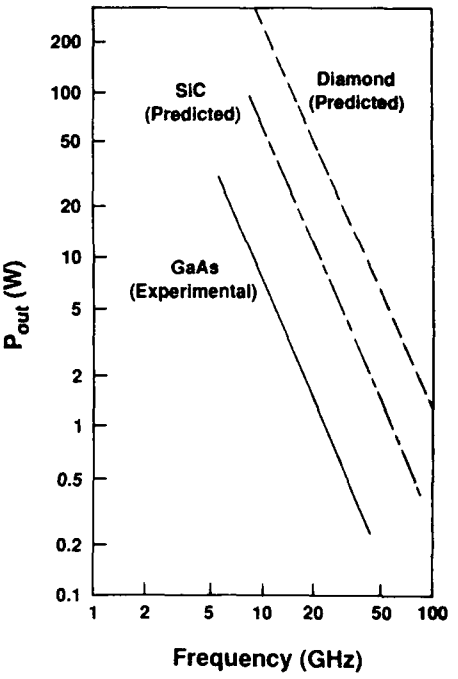

Fig. 15. RF power performance versus frequency for diamond, SiC, and GaAs MESFET's.

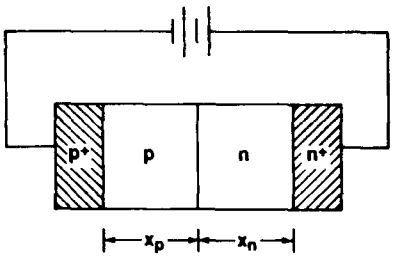

Fig. 16. Double-drift IMPATT diode structure.

the necessary bulk semiconductor and contact regions. If charge carrier mobility is too low, the semiconductor may reach dielectric breakdown conditions before the saturation field can be achieved.

IMPATT diode structures in Si, InP, GaAs, and diamond were designed [98]. The various diodes were optimized by adjusting dopant levels and layer thicknesses until a peak dc to RF conversion efficiency for each diode at each frequency of interest was obtained. Operation at 35, 44, 60, and 94 GHz was considered. All diodes were operated at the same current density for each frequency. Bias current density scales with frequency and for this study the bias current densities are 10, 12, 20, and 40 kA/cm^2 for the indicated frequencies. The design parameters for the diamond IMPATT diodes are listed in Table 4 along with the calculated breakdown voltages.

The RF output power as a function of frequency calculated for the diamond IMPATT diodes are compared in Fig. 17 to experimental data for IMPATT diodes fabricated from

Table 4 Diamond IMPATT Diode Design Parameters

Frequency (GHz)	$N_a(cm^{-3})$	$N_d(cm^{-3})$	x_p (μm)	x_n (μm)	V_B
35	1.1×10^{16}	9.0×10^{15}	1.80	2.20	235
44	1.5×10^{16}	1.2×10^{16}	1.50	1.80	208
60	2.2×10^{16}	1.8×10^{16}	1.00	1.2	146
94	3.6×10^{16}	3.1×10^{16}	0.80	0.90	124

GaAs, Si, and InP. The numbers next to the plotted points indicate the dc-to-RF conversion efficiencies obtained. The diamond IMPATT is predicted to be capable of producing about 10 W RF power with 22–23% efficiency at 30–40 GHz. This is approximately five times the power capability of comparable Si and GaAs IMPATT's, although the conversion efficiencies are essentially equivalent. The diamond IMPATT has superior RF output power capability up to about 100 GHz. At 100 and 220 GHz, the diamond IMPATT is predicted to produce 1.5 W with 10% efficiency and 60 mW with 3% efficiency, respectively. The RF performance degrades above 100 GHz and is approximately the same as Si IMPATT's up to about 220 GHz. The degradation in RF power of the diamond IMPATT above 100 GHz is due to spreading of the avalanche region. That is, as the device length is reduced for higher frequency operation the avalanche region occupies an increasingly larger proportion of the total diode length, thereby degrading the device negative resistance. Optimum IMPATT operation is obtained when the avalanche region is restricted to a small portion of the total diode length. However, due to the ionization characteristics of electrons and holes in diamond it is difficult to restrict the region over which avalanche occurs. It is difficult to design IMPATT's for operation at significantly higher frequencies than indicated.

The dc-to-RF conversion efficiencies for IMPATT's fabricated from several materials are shown in Fig. 18. The conversion efficiencies for Si, GaAs, and diamond are approximately equivalent over a frequency range extending from 35 to 95 GHz, although the efficiency of the InP IMPATT is significantly higher and demonstrates less degradation with frequency.

An investigation of the RF performance of SiC IMPATT's produces results that lie between those for Si and diamond, in agreement with the calculations reported by Mehdi *et al.* [101]. At around 100 GHz, the RF power performance for a SiC IMPATT is essentially equivalent to that for a Si diode, but the conversion efficiency is less than obtained for the diamond device (i.e., less than approximately 10%). Below 100 GHz SiC IMPATT's are capable of improved RF output power compared to Si and GaAs devices, but have reduced RF power capability compared to diamond devices. At 20–30 GHz, a SiC IMPATT is capable of producing about 4 W RF power with a conversion efficiency of about 15–20%. The high frequency performance of SiC IMPATT's is limited by relatively large series resistance due to the low carrier mobility. It will be difficult to take advantage of the double-drift structure, especially with α-SiC, due to the low hole mobility. A SiC IMPATT will probably need to be fabricated as a single drift region device to eliminate the large series resistance associated with p-type material. Low carrier mobility and the corresponding large parasitic series resistance become increasingly limiting as the device is scaled for high frequency operation. High frequency devices must have their area scaled inversely to operating wavelength, and this, in turn, enhances the magnitude of the series resistance due to aspect ratio considerations. For this reason, conversion efficiency degrades rapidly with frequency and SiC IMPATT's will, most likely, by limited to microwave applications.

C. Bipolar Transistors

Preliminary bipolar transistors have been reported in diamond [64], [67]. These devices were limited in RF performance by available technology. In particular, the technology required to fabricate a complex, multilayered structure such as the BJT does not presently exist. These early devices, however, indicate the bipolar devices are possible in diamond. Preliminary bipolar transistors have also been reported in α-SiC [11] with current gains in the range of $\beta \sim 4$–8. In the work reported here, the RF performance of SiC bipolar transistors is investigated.

The RF power performance of bipolar transistors fabricated from α-SiC was simulated using commercially available software [99]. The simulator permits the RF performance of devices to be investigated by the use of equivalent circuit techniques. Equivalent circuit parameter values are determined for specified bias and operating conditions and then used as input data for the model. The dc and RF circuits and the input RF conditions (input power drive and frequency) must also be supplied. The simulator returns RF output power at the fundamental and harmonics. Knowledge of the RF output power, along with the defined input power and dc bias conditions permits the RF gain and power-added efficiency to be determined.

The design of the bipolar transistor was accomplished using an iterative procedure beginning with assumed geometry and doping concentrations. For this investigation doping densities are selected based upon technologically achievable limits. That is, doping densities are limited to those possible with currently available epitaxial growth and doping technology. An initial estimate for the device geometry can be determined from impedance matching considerations, subject to distributed effects limitations. Since operation at low microwave frequency will allow large device size it is necessary to use multiple emitter

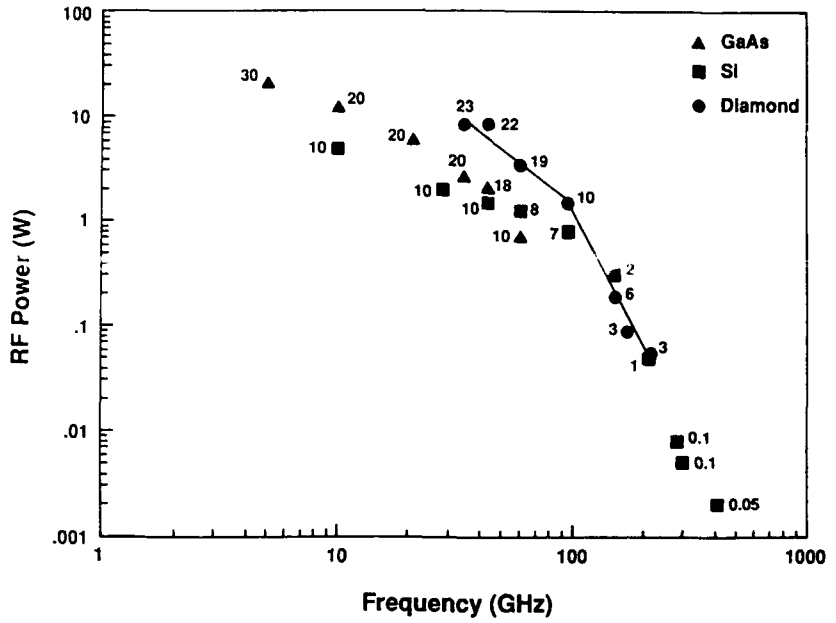

Fig. 17. RF output power versus frequency for various IMPATT diodes.

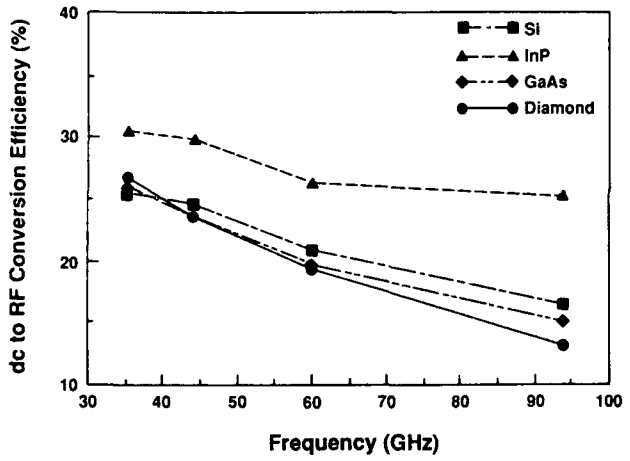

Fig. 18. Conversion efficiency versus frequency for IMPATT diodes fabricated from various semiconductors.

fingers. The length of each finger will vary according to the design frequency, but in general will be subject to the 1/20 λ restriction discussed in the MESFET section. The cross-section of the final device design is shown in Fig. 19 and the design parameters are listed in Table 5. The device was designed for 10 GHz operation and has a total of eight emitter fingers. The number of emitter fingers was selected based upon impedance matching and emitter current density considerations. As the base-emitter junction area is increased the input impedance decreases. BJT's fabricated from SiC, however, will have a relatively large base resistance and this factor will ultimately dominate the input impedance. Under these conditions the device area will be limited by emitter current density and output port impedance matching considerations. It is desirable to keep the device output impedance in the range of 25–50 Ω and the emitter current density in the range of 20–30 kA/cm^2. The most critical design considerations were directed toward the base and collector region. Base region design issues include the conflicting effects of base region resistance and base region transit time. Collector region design issues include base-collector region capacitance (charge storage) and base-collector depletion region transit time. The base region design involves a calculation of the current gain, base resistance, and base region transit-time. The current gain is calculated from consideration of minority carrier transport across the base region. In the common-base configuration, the dc current gain is defined as α_0 and is given by the expression

$$\alpha_0 = \frac{1}{\cosh\left(\frac{W_B}{L_B}\right) + \frac{D_{pE} L_B N_B}{D_{nB} L_E N_E} \sinh\left(\frac{W_B}{L_B}\right)} \tag{4}$$

where the various terms are calculated from the design dimensions listed in Table 5. Base region transit-time τ_B is also an important factor and this parameter is generally defined in terms of the alpha cutoff frequency for the device defined as

$$f_\alpha = \frac{1}{2\pi\tau_B} = \frac{D_{nB}}{\pi W_B^2}. \tag{5}$$

The dc current gain will degrade with frequency according to the expression

$$\alpha = \frac{\alpha_0 e^{-j\omega\tau_c}}{1 + j\frac{f}{f_c}} \tag{6}$$

where the various terms are indicated in Table 6. These expressions indicate the tradeoffs between base region and base-collector region transit-times in determining the current gain for the device.

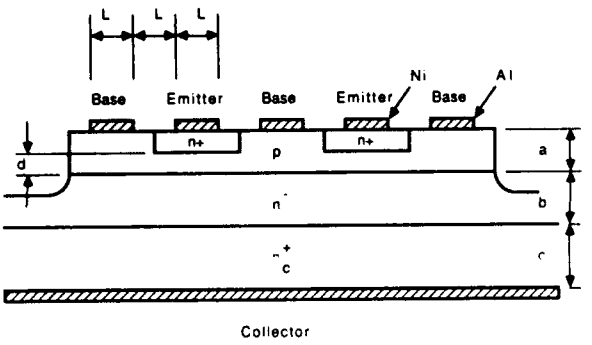

Fig. 19. Cross section of a SiC bipolar transistor.

Table 5 SiC Transistor Dimensions

Parameter	Dimension
L	2 μm
a	0.5 μm
b	5 μm
c	50 μm
d	0.2 μm
n^+	2×10^{19} cm^{-3}
p	3×10^{18} cm^{-3}
n^-	8×10^{15} cm^{-3}
n_c^+	4×10^{17} cm^{-3}
R_c(E)	5×10^{-5} $\Omega - cm^2$
R_c(B)	7×10^{-4} $\Omega - cm^2$
R_c(C)	10^{-3} $\Omega - cm^2$

The base thickness is W_B=0.2 μm. For this base thickness a value of α_0=0.894 is obtained, which results in a common-emitter current gain of β_0=8.4. This is low according to Si BJT standards where α_0 is typically greater than 0.95 and β_0 greater than 20. The parameters listed in Table 5 yield a base resistance value of 29.7 Ω for the 8 emitter finger device. Selection of the base region thickness and doping concentration is a critical design factor for the device. As base region thickness is reduced α_0 increases and base region transit-time decrease, enhancing performance, but base resistance increases, thereby degrading performance. An increase in base region doping reduces base resistance, but decreases α_0 and base-region transit-time.

Tradeoffs involved in collector region design are directed toward base-collector region capacitance, C_{BC}, and base-collector depletion region transit-time, τ_C. An increase in collector doping decreases the base-collector depletion region and corresponding transit-time, but increases collector capacitance. An increased collector capacitance lowers output impedance, thereby limiting device area. The base-collector depletion region transit-time introduces an inductive delay that degrades RF performance.

Table 6 Element Values

Parameter	Value
No. Emitter Fingers	8
Vce	150 v
I_{ce}	1 A
BV_{ce}	346 v
R_B	29.7 Ω
R_{BE}	0.05 Ω
C_{BE}	15.92 pF
$C_{BE(0)}$	11.93 pF
R_E	2.5 Ω
C_{BC}	0.184 pF
$C_{BC(0)}$	1.5 pF
R_{BC}	250 Ω
R_C	6.4 Ω
α_0	0.894
β_0	8.4
f_α	23.7 GHz
τ_c	23 pS
$\tau_{(minority\ lifetimes)}$	10 nS

The large-signal equivalent circuit model for the BJT used in this work is shown in the common-emitter configuration in Fig. 20. This is a standard model for the bipolar transistor and contains elements of most significance to the RF operation of the device. The calculated parameter values are listed in Table 6. Package and lead parasitic elements were added to make the simulations more physical. For this work the common-emitter configuration and class A operating conditions were chosen. Power devices can be operated either in common-emitter or common-base configurations. A common-base configuration is generally used when the device is limited in RF performance by breakdown voltage considerations. Since SiC has a large critical field for breakdown, collector breakdown voltage limitations are not expected to be a factor and for this reason the more desirable common-emitter configuration is selected.

The RF performance as a function of frequency for the SiC BJT is shown in Fig. 21. At frequencies above about 1.5 GHz the RF output power and gain degrade at a -3 dB/octave rate. The PAE degrades rapidly with frequency and the device will not produce useful power above approximately 4 GHz. Below 1.5 GHz the RF output power of the device is essentially constant, indicating that the device design is probably not optimum for low frequency operation. At these frequencies, the device area

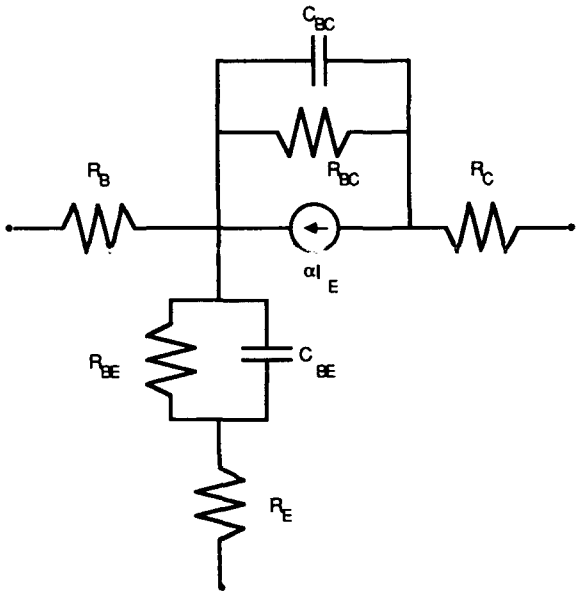

Fig. 20. Equivalent circuit for a SiC bipolar transistor.

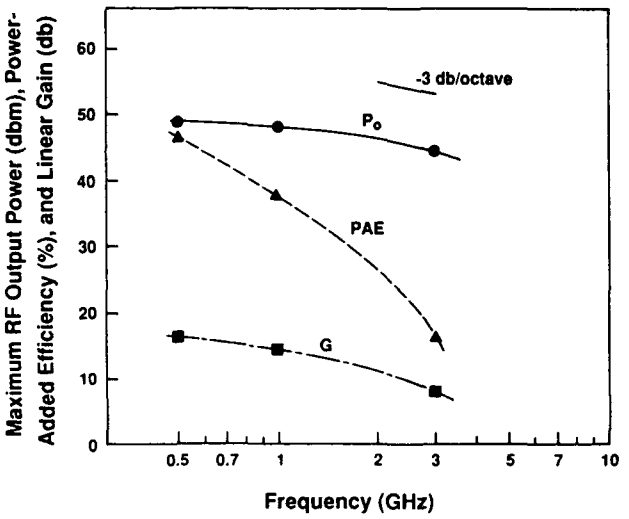

Fig. 21. RF output power versus frequency for SiC bipolar transistors.

could possibly be increased to increase output power. Attempts to design such a device, however, were not successful due to impedance matching problems introduced by increased collector capacitance and conductance with large area devices.

V. Summary And Conclusions

The suitability of using SiC and diamond for fabrication of high frequency electronic devices has been investigated. The analysis consisted of theoretical calculations of the power performance of MESFET, IMPATT, and bipolar transistor device structures. Operation at microwave and millimeter-wave frequencies was considered. The MESFET is an attractive microwave device for implementation in wide bandgap semiconductor due to its simple structure, ease of fabrication and excellent RF performance. The investigation revealed that MESFET's fabricated in both SiC and diamond may produce microwave and mm-wave devices with superior RF power capability compared to similar devices fabricated from commonly used semiconductors such as GaAs and Si. Diamond MESFET's are capable of producing over 200 W of *X*-band power as compared to about 8 W for GaAs MESFET's. Devices fabricated from SiC should perform between these limits. A SiC MESFET will not perform as well as a diamond device due to a larger thermal resistance, a larger dielectric constant, and a lower charge carrier mobility. Diamond MESFET's may be capable of producing approximately 1 W of RF power at 100 GHz. Diamond and SiC IMPATT diodes also are capable of producing improved RF power compared to Si, GaAs, and InP devices at microwave frequencies. RF performance degrades with frequency and only marginal improvements are indicated at mm-wave frequencies. Bipolar transistors fabricated from wide bandgap material probably offer improved RF performance only at UHF and low microwave frequencies.

The realization of the predicted performance requires that significant advances be made in material growth and doping and contact technology in both SiC and diamond. Diamond technology, in particular, must be significantly improved if devices are to be realized. The calculations presented here assumed n-type diamond with activated donors of specified density. The n-type material was investigated because its properties yield the highest performance devices and the investigation was directed toward defining the ultimate performance potential of the devices. In fact, device quality n-type crystals have not yet been produced and it is not known if suitable donors for producing n-type diamond exist. Obviously, if material technology cannot be successfully developed electronic devices of significance will not be possible. These calculations do, however, indicate the potential payoff from a successful material technology. If suitable crystals can be produced, properly designed and fabricated devices have the potential to significantly improve the RF operation of high frequency devices over that available from devices fabricated from competing semiconductors. The development of diamond devices, in particular, will represent a significant improvement in the state-of-the-art. The future for SiC devices is more apparent. The material technology is rapidly progressing and device performance is improving. SiC diodes, LED's, and MESFET's will most likely find commercial applications. It is expected that the wide bandgap semiconductors will be useful in power applications where the combination of high carrier velocity and thermal conductance provide an advantage not available with Si or compound semiconductor devices. Device structures most likely to benefit from SiC and diamond are those that operate in velocity saturation since these devices minimize the degrading effects of low carrier mobility.

References

[1] R. Robertson, J. J. Fox, and A. E. Martin, "Two types of diamond," *Phil. Trans. Roy. Soc.*, vol. A232, pp. 463–469, Mar. 1934.

[2] H. Jagodzinski and H. Arnold, "The Crystal Structure of Silicon Carbide," in *Silicon Carbide, A High-Temperature Semiconductor,* J. R. O'Connor and J. Smiltens, Eds. New York: Pergamon, 1960, pp. 136–145.

[3] N. W. Jepps and T. F. Pagae, "Crystal growth and characterization of polytype structures," *Progress in Crystal Growth and Characterization,* vol. 7, p. 259, 1983.

[4] J. A. Powell, "Silicon carbide: Progress in crystal growth," *Mater. Res. Soc. Symp. Proc.*, vol. 97, 1987.

[5] A. G. Acheson, British Patent 17911, 1892.

[6] A. Lely, "Darstellung von Einkristallen von Silizium Carbid und Bekerrschung von Art and Meng der Eingebauten Verunreinigunger," *Ber. Deut. Keram. Ges.*, vol. 32, pp. 229–231, 1955.

[7] H. J. Kim and R. F. Davis, "Physical and chemical nature of films formed on Si(100) surfaces subjected to C_2H_4 at elevated temperatures," *J. Electrochem. Soc.*, vol. 134, pp. 2269–2275, Sept. 1987.

[8] R. F. Davis, Z. Sitar, B. E. Williams, H. S. Kong, H. J. Kim, J. W. Palmour, J. A. Edmond, J. Ryu, J. T. Glass, and C. H. Carter, "Critical evaluation of the status and the areas for future research regarding the wide bandgap semiconductors of diamond, gallium-nitride, and silicon sarbide," *Mat. Sci. Eng.*, vol. B1, pp. 77–104, Jan. 1988.

[9] L. J. Kroko and A. G. Milnes, "Diffusion of nitrogen into silicon carbide single crystals doped with aluminum," *Solid-State Electron.*, vol. 9, pp. 1125–1134, 1966.

[10] G. Kelner, S. Binari, K. Sleger, and H. Kong, "β-SiC MESFET's and buried-gate JFET's," *IEEE Electron Device Lett.*, vol. EDL-8, pp. 428–430, Sept. 1987.

[11] W. V. Muench, P. Hoeck, and E. Pettenpaul, "Silicon carbide field-effect and bipolar transistors," in *1977 IEEE Int. Electron Device Meeting Dig.*, pp. 337–339.

[12] S. Shibahara, T. Saito, S. Nishino, and H. Matsunami, "Fabrication of inversion-type n-channel MOSFET's using cubic-SiC on Si(100)," *IEEE Electron Device Lett.*, vol. EDL-7, pp. 692–693, Dec. 1986.

[13] J. W. Bumgarner, H. S. Kong, H. J. Kim, J. W. Palmour, J. A. Edmond, J. T. Glass, and R. F. Davis, "Monocrystalline β-SiC semiconductor thin films: Epitaxial growth, doping and FET device development," in *1988 Proc. 38th Electronics Components Conf.*, pp. 342–349.

[14] R. F. Davis, "Epitaxial growth and doping of and device development in monocrystalline β-SiC semiconductor thin films," *Thin Solid Films,* vol. 181, pp. 1–15, Dec. 1989.

[15] M. Yamanaka, H. Daimon, E. Sakuma, S. Misawa, and S. Yoshida, "Temperature dependence of electrical properties of n- and p-type 3C-SiC," *J. Appl. Phys.*, vol. 61, pp. 599–603, Jan. 1987.

[16] H. J. Round, "A note on carborundum," *Elec. World,* vol. 49, p. 309, Feb. 1907.

[17] R. W. Brander and R. P. Sutton, "Solution grown SiC p-n junctions," *J. Phys. D: Appl. Phys.*, vol. 2, pp. 309–318, Mar. 1969.

[18] W. V. Muench and E. Pettenpaul, "Saturated electron drift velocity in 6H silicon carbide," *J. Appl. Phys.*, vol. 48, pp. 4823–4825, Nov. 1977.

[19] S. Yoshida, H. Daimon, M. Yamanaka, E. Sakuma, and K. Endo, "Schottky-barrier field-effect transistors of 3C-SiC," *J. Appl. Phys.*, vol. 60, pp. 2989–2991, Oct. 1986.

[20] H. Daimon, M. Yamanaka, M. Shinohara, E. Sakuma, S. Misawa, K. Endo, and S. Yoshida, "Operation of Schottky-barrier field-effect transistors of 3C-SiC up to 400°C," *Appl. Phys. Lett.*, vol. 51, pp. 2106–2108, Dec. 1987.

[21] H. S. Kong, J. W. Palmour, J. T. Glass, and R. F. Davis, "Temperature dependence of the current-voltage characteristics of metal-semiconductor field-effect transistors in n-type β-SiC grown via chemical vapor deposition," *Appl. Phys. Lett.*, vol. 51, pp. 442–444, Aug. 1987.

[22] G. Kelner, S. Binari, K. Sleger, and H. Kong, "β-SiC MESFET's and buried-gate JFET's," *IEEE Electron Device Lett.*, vol. EDL-8, pp. 428–430, Sept. 1987.

[23] ——, "β-SiC MESFET's," *Mater. Res. Soc. Symp. Proc.*, vol. 97, pp. 227–232, 1987.

[24] K. Furukawa, A. Hatano, A. Uemoto, Y. Fujii, K. Nakanishi, M. Shigeta, A. Suzuki, and S. Nakajima, "Insulated-gate and junction-gate FET's of CVD-grown β-SiC," *IEEE Electron Device Lett.*, vol. EDL-8, pp. 48–49, Feb. 1987.

[25] G. Kelner, M. S. Shur, S. Binari, K. J. Sleger, and H. S. Kong, "High-transconductance β-SiC buried-gate JFET's," *IEEE Trans. Electron Devices,* vol. 36, pp. 1045–1049, June 1989.

[26] J. W. Palmour, "α-SiC MESFETs" presented at the 1990 WOCSEMMAD Conf., San Francisco, CA.

[27] J. F. H. Custers, "Unusual phosphorescence of a diamond," *Physica,* vol. 18, pp. 489–496, Aug./Sep. 1952.

[28] C. M. Huggins and P. Cannon, "Diamond containing controllable impurity concentrations," *Nature,* vol. 194, pp. 829–830, June 1962.

[29] R. H. Wentorf, "Preparation of semiconducting diamonds," *J. Chem. Phys.*, vol. 36, pp. 1987–1990, April, 1962.

[30] B. V. Derjaguin and D. V. Fedoseev, "The synthesis of diamond at low pressure," *Sci. Amer.*, vol. 233, pp. 102–109, Nov. 1975.

[31] B. V. Spitsyn, L. L. Bouilov, and B. V. Derjaguin, "Vapor growth of diamond on diamond and other surfaces," *J. Cryst. Growth,* vol. 52, pp. 219–226, Apr. 1981.

[32] R. Mania, L. Strobierski, and R. Pampuch, "Diamond synthesis in cool plasma," *Cryst. Res. Technol.*, vol. 16, pp. 785–788, July 1981.

[33] S. Matsumoto, Y. Sato, and M. Tsutsumi, "Growth of diamond particles from methane-hydrogen," *J. Mater. Sci.*, vol. 17 pp. 3106–3112, Nov. 1982.

[34] S. Matsumoto, Y. Sato, M. Kamo, J. Tanaka, and N. Setaka, in *Proc. 7th Int. Conf. Vacuum Metallurgy,* Iron and Steel Institute of Japan, Tokyo, Japan, 1982, p. 386.

[35] S. Matsumoto, Y. Matsui, "Electron microscopic observation of diamond particles grown from the vapor phase," *J. Mater. Sci.*, vol. 18, pp. 1785–1793, June 1983.

[36] K. Kobashi, K. Nishimura, Y. Kawate, and T. Horiuchi, in *34th Nat. Symp. American Vacuum Society,* Anaheim, CA, Nov. 2–6, 1987.

[37] B. E. Williams, J. T. Glass, R. F. Davis, K. Kobashi, and T. Horiuchi, presented at the *34th National Symp. American Vacuum Society,* Anaheim, CA, Nov. 1987, paper #TG-WeA9, p. 37.

[38] M. Kamo, Y. Sato, S. Matsumoto, and N. Setaka, "Diamond synthesis from gas phase in microwave plasma," *J. Cryst. Growth,* vol. 62, pp. 642–644, Aug. 1983.

[39] Y. Mitsuda, Y. Kojima, T. Yoshida, and K. Akashi, "The growth of diamond in microwave plasma under low pressure," *J. Mater. Sci.*, vol. 22, pp. 1557–1562, May 1987.

[40] S. Matsumoto, in *Proc. 7th Int. Symp. Plasma Chemistry* (Elmsford, NY), C.J. Timmermans, Ed. Eindhoven, The Netherlands: Pergamon, July 1985, vol. 1, p. 79.

[41] S. Matsumoto, "Chemical vapor deposition of diamond in RF glow discharge," *J. Mater. Sci. Lett.*, vol. 4, pp. 600–602, May 1985.

[42] A. Sawabe and T. Inuzuka, "Growth of diamond thin films by electron assisted chemical vapor deposition," *Appl. Phys. Lett.*, vol. 46, pp. 146–147, Jan. 1985.

[43] ——, "Growth of diamond thin films by electron-assisted chemical vapor deposition and their characterization," *Thin Solid Films,* vol. 137, pp. 89–99, Mar. 1986.

[44] K. Kitahama, "Synthesis of diamond by laser-induced chemical vapor deposition," *Appl. Phys. Lett.*, vol. 49, pp. 634–635, Sept. 1986.

[45] M. Kitabatake and K. Wasa, "Growth of diamond at room temperature by an ion-beam sputter deposition under hydrogen bombardment," *J. Appl. Phys.*, vol. 25, pp. 1693–1695, Aug. 1985.

[46] J. E. Shigley, E. Fritsch. C. M. Stockton, J. I. Koivula, C. W. Fryer, and R. E. Kane, "The gemological properties of the sumitomo gem-quality synthetic yellow diamonds," *Gems and Gemology,* vol. 22, pp. 192–208, 1986.

[47] S. Yazu, "Properties and applications of high pressure synthesized diamond single crystals", presented at the *Diamond Technology Initiative Symp.*, Crystal City, VA, July 1989, paper TH9.

[48] J. E. Shigley, E. Fritsch, C. M. Stockton, J. I. Koivula, C. W. Fryer, and R. E. Kane, *Gems and Gemology,* vol. 23, pp. 187–206, 1987.

[49] V. S. Vavilov, M. I. Guseva, E. A. Konorova, and V. F.

Sergienko, "Investigation of the Hall Effect in p-type semiconducting diamond doped with boron by the ion implantation method," *Sov. Phys.—Semicond.*, vol. 4, pp. 12–16, July 1970.
[50] V. S. Vavilov, M. I. Guseva, E. A. Konorova, and V. F. Sergienko, "Investigation during isochronous multstage annealing of the electrical conductivity of semiconducting n- and p-type diamonds prepared by the ion implantation method," *Sov. Phys.—Semicond.*, vol. 4, pp. 6–11, July 1970.
[51] V. S. Vavilov, M. A. Gukasya, M. I. Guseva, T. A. Karatygia, and E. A. Konorova, "Some electrical properties of diamond doped by implantation of boron ion," *Sov. Phys.—Semicond.*, vol. 8, pp. 471–473, Oct. 1974.
[52] J. F. Prins, "Activation of boron-dopant atoms in ion-implanted diamonds," *Phys. Rev. B*, vol 38, pp. 5576–5584, Sept. 1988.
[53] ——, "Improved activation of boron-doped atoms implanted into diamond," *Nuclear Instrum. Methods in Physics Research*, vol. B35, pp. 484–487, 1988.
[54] ——, "Fermi-dirac statistics and the nature of the compensating donors in boron-doped diamond layers," *Phys. Rev. B*, vol. 39, pp. 3764–3770, Feb. 1989.
[55] V. S. Vavilov, M. A. Gukasya, M. I. Guseva, T. A. Karatygia, and E. A. Konorova, "Conductivity of diamond doped by implantation of phosphorus ions," *Sov. Phys.—Semicond.*, vol. 9, pp. 962–964, 1976.
[56] V. S. Vavilov, E. A. Konorova, E. B. Stepanova, and E. M. Trukhan, "Infrared photoconductivity of diamond doped by implanting lithium ions," *Sov. Phys.—Semicond.*, vol. 13, pp. 604–606, May 1979.
[57] ——, "Electrical properties of diamond doped by implantation of lithium ion," *Sov. Phys.—Semicond.*, vol. 13, pp. 635–638, June 1979.
[58] V. S. Vavilov, M. A. Gukasya, E. A. Konorova and Y. U. Milyutin, "Implantation of antimony ions into diamond," *Sov. Phys.—Semicond.*, vol. 6, pp. 1998–2002, June 1973.
[59] N. Fujimori, T. Imai and A. Doi, "Characterization of conducting diamond films," *Vacuum*, vol. 36, no. 1–3, pp. 99–102, 1986.
[60] K. Okano, H. Naruki, Y. Akiba, T. Kurosu, M. Iida, and Y. Hirose, "Synthesis of diamond thin films having semiconductor properties," *Japan. J. Appl. Phys.*, vol. 27, pp. L173–L175, Feb. 1988.
[61] V. K. Bazhenov, I. M. Bikulin, and A. G. Gontar, "Synthetic diamonds in electronics (review)," *Sov. Phys.—Semicond.*, vol. 19, pp. 829–841, Aug. 1985.
[62] A. S. Brown, "Diamonds shine brightly in aerospace's future," *Aerospace America*, pp. 12–15, Nov. 1987.
[63] G. B. Rodger and F. A. Raal, "Semiconducting diamonds as thermistors," *Rev. Sci. Instrum.*, vol. 31, pp. 663–664, 1960.
[64] J. F. Prins, "Bipolar transistor action in implanted diamond," *Appl. Phys. Lett.*, vol. 41, pp. 950–952, Nov. 1982.
[65] G. H. Glover, "The C-V characteristics of Schottky Barriers on laboratory grown semiconducting diamonds," *Solid-State Electron.*, vol. 16, pp. 973–983, 1973.
[66] L. F. Vereshchagin, K. K. Demidov, O. G. Revin, and V. N. Slesarev, "Thermistor made of p-type synthetic diamond," *Sov. Phys.—Semicond.*, vol. 8, pp. 1581–1582, June 1975.
[67] M. W. Geis, D. D. Rathman, D. J. Ehrlich, R. A. Murphy, and W. T. Lindley, "High-temperature point-contact transistors and Schottky diodes on synthetic boron-doped diamond," *IEEE Electron Device Lett.*, vol. EDL-8, pp. 341–343, Aug. 1987.
[68] G. S. Gildenblat, S. A. Grot, C. R. Wronski, A. R. Badzian, T. Badzian, and R. Messier, "Electrical characteristics of Schottky diodes fabricated using plasma assisted chemical vapor deposited diamond films," *Appl. Phys. Lett.*, vol. 53, pp. 586–588, Aug. 1988.
[69] Y. Tzeng, T. H. Lin, J. L. Davidson, and L. S. Lan, "Fabrication and high temperature characteristics of diamond electronic devices," in *1987 University/Government/Industry Microelectronics Symp.*, 1987, pp. 187–190.
[70] M. I. Guseva, E. A. Konorova, Y. A. Kuznetsov, and V. F. Sergienko, "Double injection of carriers in a p-i-n structure made of implantation-doped diamond," *Sov. Phys.—Semicond.*, vol. 12, pp. 290–293, Mar. 1978.
[71] H. Shiomi, Y. Nishibayaski, and N. Fujimori, "Field-effect transistors using boron-doped diamond epitaxial films," *Japan. J. of Appl. Phys.*, vol. 28, pp. L2153–L2154, Dec. 1989.
[72] W. Tsui, M. Delfino, D. Hodul, M. Riaziat, L. Y. Ching, G. Reynolds and C. B. Cooper, "Diamond MESFET using ultrashallow RTP boron doping," *IEEE Electron Device Lett.*, vol. 12, pp. 157–159, Apr. 1991.
[73] A. T. Collins, "Diamond electronic devices—A critical appraisal," *Semicond. Sci. Technol.*, vol. 4, pp. 605–611, 1989.
[74] D. K. Ferry, "High-field transport in wide-bandgap semiconductors," *Phys. Rev. B*, vol. 12, pp. 2361–2369, Sept. 1975.
[75] C. Canali, E. Gatti, S. F. Kozlov, P. F. Manfredi, C. Manfredottti, F. Nava, and A. Quirini, "Electrical properties and performances of natural diamond nuclear radiation detectors," *Nuclear Instrum. and Methods*, vol. 160, pp. 73–77, 1979.
[76] M. A. Osman, G. Andrews, J. P. Kreskovsky, and H. L. Grubin, "Numerical simulation studies of semiconducting diamond electronic devices," Final Report on Contract DNA001-87-C-0250, Defense Nuclear Agency, Feb. 1989.
[77] F. Nava, C. Canali, C. Jacoboni, L. Reggiani, and S. F. Kozloz, "Electron effective masses and lattice scattering in natural diamond," *Solid State Commun.*, vol. 33, pp. 475–477, Jan. 1980.
[78] W. V. Muench and E. Pettenpaul, "Saturated electron drift velocity in 6H silicon carbide," *J. Appl. Phys.*, vol. 48, pp. 4823–4825, Nov. 1977.
[79] M. E. Levinshtein and E. I. Radovanova, "Characterization of the drift velocity of electrons in silicon carbide subjected to strong electric fields," *Sov. Phys.—Semicond.*, vol. 11, pp. 232–234, Feb. 1977.
[80] S. Nishomo, H. Suhara, and H. Matsunami, "Reproducible preparation of cubic-SiC single crystals by chemical vapor deposition," in *Extended Abstracts of the 15th Conf. Solid State Devices and Materials*, Tokyo, Japan, 1983, pp. 317–320.
[81] R. A. Rudder, G. C. Hudson, M. J. Mantini, and R. B. Markunas, "Low pressure deposition of diamond films using H_2 RF discharges containing CH_4 and CO," presented at the Diamond Technology Initiative Symp., Crystal City, VA, 1989, p. T16.
[82] E. A. Konorova, Y. A. Kuznetsov, V. F. Sergienko, S. D. Tkachenko, A. V. Tsikunov, A. V. Spitsyn, and Y. Z. Danyushevski, "Impact ionization in semiconductor structures made of ion-implanted diamond," *Sov. Phys.—Semicond.*, vol. 17, pp. 146–149, Feb. 1983.
[83] P. Liu, R. Yen, and N. Bloembergen, "Dielectric breakdown threshold, two-photon absorption, and other optical damage mechanisms in diamond," *IEEE J. Quantum Electron.*, vol. QE-14, pp. 574–576, Aug. 1978.
[84] G. H. Glover, "Charge multiplication in Au-SiC(6H) Schottky junctions," *J. Appl. Phys.*, vol. 46, pp. 4842–4844, Nov. 1975.
[85] C. van Opdorp and J. Vrakking, "Avalanche breakdown in epitaxial SiC p-n junctions," *J. Appl. Phys.*, vol. 40, pp. 2320–2322, Apr. 1969.
[86] A. P. Dmitriev, A. O. Konstantinov, D. P. Litvin, and V. I. Sankin, "Impact ionization and superlattice in 6H-SiC," *Sov. Phys.—Semicond.*, vol. 17, pp. 686–689, June 1983.
[87] M. M. Anikin, M. E. Levinshtein, I. V. Popov, V. P. Rastegaev, A. M. Strel'chuk, and A. L. Skyrkin, "Temperature dependence of the avalanche breakdown voltage of silicon carbide p-n junctions," *Sov. Phys.—Semicond.*, vol. 22, pp. 995–998, Sept. 1988.
[88] C. R. Crowell and S. M. Sze, "Temperature dependence of avalanche multiplication in semiconductors," *Appl. Phys. Lett.*, vol. 9, pp. 242–244, Sept. 1966.
[89] J. W. Palmour, Cree Research, Triangle Park, NC, private communication.
[90] M. D. Bell and W. J. Leivo, "Rectification, photoconductivity, and photovoltaic effect in semiconducting diamond," *Phys. Rev.*, vol. 111, pp. 1227–1231, Nov. 1958.
[91] F. J. Himpsel, P. Heimann, and D. E. Eastman, "Schottky barriers on diamond (111)," *Solid State Commun.*, vol. 36, pp. 631–633, Nov. 1980.
[92] S. A. Grot, G. S. Gildenblat, C. W. Hatfied, C. R. Wronski, A. R. Badzian, T. Badzian, and R. Messier, "The effect of surface treatment on the electrical properties of metal contacts to boron-doped homoepitaxial diamond film," *IEEE Electron Device Lett.*, vol. 11, pp. 100–102, Feb. 1990.
[93] V. S. Vavilov, M. A. Gukasyan, M. I. Guseva, and E. A. Konorova, "Electrical conductivity of diamond containing implanted Li ions," *Sov. Phys.—Semicond.*, vol. 6, pp. 741–746, Nov. 1972.
[94] A. T. Collins, E. C. Lightowlers, and A. W. S. Williams, "Formation of electric contacts on insulating and semiconduct-

ing diamonds," *Diamond Res.* (Suppl. Ind. *Diamond Rev.*), pp. 19–22, 1970.
[95] K. L. Moazed, R. Nguyen, and J. R. Zeidler, "Ohmic contacts to semiconducting diamond," *IEEE Electron Device Lett.*, vol. 9, pp. 350–351, July 1988.
[96] K. L. Moazed, J. R. Zeidler, M. J. Taylor, R. Nguyen, and C. R. Zeisse, "Electrical contacts to semiconducting diamond," in *Proc. 1989 high frequency power conversion international*, Naples, FL, May, 1989, pp. 117–129.
[97] M. A. Khatibzadeh and R. J. Trew, "A large-signal, analytic model for the GaAs MESFET," *IEEE Trans. Microwave Theory Tech.*, vol. MTT-36, pp. 231–238, Feb. 1988.
[98] P. M. Mock and R. J. Trew, "RF performance characteristics of double-drift MM-wave diamond IMPATT diodes," in *Proc. 1989 IEEE/Cornell Conf. Advanced Concepts in High-Speed Semiconductor Devices and Circuits*, pp. 383–389.
[99] Libra (Nonlinear Microwave Device/Circuit Simulator), EEsof, Westlake Village, CA.
100] T. Wada and J. Frey, "Physical basis of short-channel MESFET operation," *IEEE Trans. Electron Devices*, vol. ED-26, pp. 476–489, Apr. 1979.
101] I. Mehdi, G. I. Haddad, and R. K. Mains, "Microwave and millimeter-wave power generation in silicon carbide avalanche devices," *J. Appl. Phys.*, vol. 64, pp. 1533–1540, Aug. 1988.

Robert J. Trew (Fellow, IEEE) received the Ph. D. degree in electrical engineering from the University of Michigan, Ann Arbor, in 1974.

From 1974 to 1976 he was with the Watkins-Johnson Company in Palo Alto, CA where he was involved in the design and development of various microwave solid-state components. In 1977, he joined the faculty of North Carolina State University, Raleigh, where he is currently Professor of electrical and computer engineering and Director of the High Frequency Electronics Laboratory. His research interests are in microwave/millimeter-wave solid-state device modeling, microwave device and circuit design, and high frequency experimental characterization, and parameter extraction techniques.

Dr. Trew is a member of Eta Kappa Nu, Sigma Xi, Tau Beta Pi, and the American Association for the Advancement of Science. He is also a member of the Electromagnetics Academy.

Jing-Bang Yan (Member, IEEE) received the B.S. degree in physics in 1982 from National Taiwan University, Taiwan, ROC, and the M.S. degree in electrical engineering in 1987 from North Carolina State University, Raleigh. He is a Ph.D. candidate in electrical engineering and is a Research Assistant in the High Frequency Electronics Laboratory in the Electrical and Computer Engineering Department at North Carolina State University.

His research interests are in the areas of modeling, computer-added design, and characterization of microwave solid-state devices.

Mr. Yan is a member of Eta Kappa Nu and Pi Mu Epsilon.

Philip M. Mock (Member, IEEE) received the B.S. degree in physics from the University of Notre Dame in 1977 and the M.S. degree in materials engineering from North Carolina State University, Raleigh in 1980. He is currently completing requirements for the Ph.D. degree in electrical engineering.

He has beer involved in GaAs FET and IMPATT development and millimeter-wave oscillator circuit design.